Cell Metabolism

Article

FGF21 reduces ER stress by enhancing the unfolded protein and integrated stress responses through increased sulfide signaling

Graphical abstract

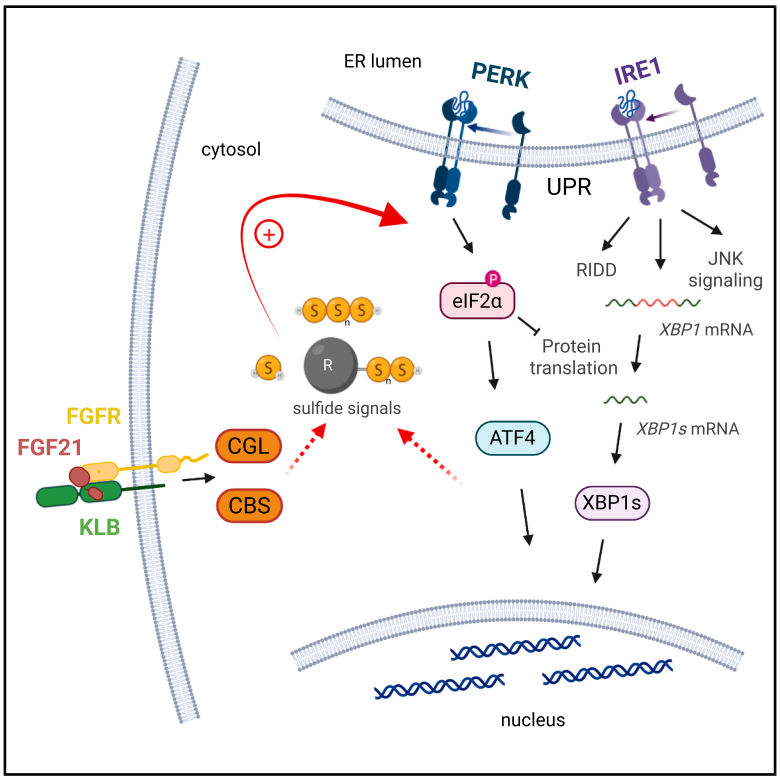

Highlights

- FGF21 enhances the UPR and ISR by increasing enzymatic sulfide production
- Sulfide signals (SSs) are also induced by the UPR independently of FGF21
- FGF21 and SSs do not initiate the UPR and ISR but enhance the stress-induced response
- FGF21 action increases cellular stress resilience and reduces ER stress chronically

Authors

Gerald Grandl, Ann-Christine König, Fabian Metzger, ..., Stefanie M. Hauck, Matthias H. Tschöp, Timo D. Müller

Correspondence

gerald.grandl@helmholtz-munich.de (G.G.), timodirk.mueller@helmholtz-munich.de (T.D.M.)

In brief

Grandl et al. reveal a novel physiological role of FGF21 as a hormone of protein folding stress. They show that FGF21 enhances but does not initiate the unfolded protein response and integrated stress response via increased enzymatic sulfide production, thereby improving stress resilience and reducing ER stress.

Grandl et al., 2026, Cell Metabolism *38*, 1–13
July 7, 2026
https://doi.org/10.1016/j.cmet.2026.05.011

CellPress

Cell Metabolism

CellPress
OPEN ACCESS

Article

FGF21 reduces ER stress by enhancing the unfolded protein and integrated stress responses through increased sulfide signaling

Gerald Grandl,[1,2,*] Ann-Christine König,[3] Fabian Metzger,[3,12] Arkadiusz Liskiewicz,[1,2,4] Tanja Hefele,[1] Shelly Nason,[5] Aaron Novikoff,[1,2] Nada Al-Refaie,[1] Md Abdur Rahman,[1] Ahmed Khalil,[1,2] Qian Zhang,[1,2] Gustav Collden,[1,2] Brian Finan,[6,7] Jonathan Douros,[7,8] Kirk Habegger,[5] Alberto Cebrian-Serrano,[1] Stefanie M. Hauck,[2,3] Matthias H. Tschöp,[9,10] and Timo D. Müller[1,2,11,13,*]

[1]Institute of Diabetes and Obesity, Helmholtz Center Munich, Munich, Germany
[2]German Center for Diabetes Research (DZD), Munich, Germany
[3]Metabolomics and Proteomics Core (MPC), Helmholtz Center Munich, Munich, Germany
[4]Department of Physiology, Faculty of Medical Sciences in Katowice, Medical University of Silesia, Katowice, Poland
[5]Comprehensive Diabetes Center and Department of Medicine, Division of Endocrinology, Diabetes and Metabolism, University of Alabama at Birmingham, Birmingham, AL, USA
[6]Eli Lilly and Company, Indianapolis, IN, USA
[7]Novo Nordisk Research Center, Indianapolis, Indianapolis, IN, USA
[8]Indiana Biosciences Research Institute, Indianapolis, IN, USA
[9]Helmholtz Center Munich, Munich, Germany
[10]Ludwig-Maximilians-University (LMU), Munich, Germany
[11]Walther-Straub Institute of Pharmacology and Toxicology, LMU, Munich, Germany
[12]Deceased
[13]Lead contact
*Correspondence: gerald.grandl@helmholtz-munich.de (G.G.), timodirk.mueller@helmholtz-munich.de (T.D.M.)
https://doi.org/10.1016/j.cmet.2026.05.011

SUMMARY

Fibroblast growth factor 21 (FGF21) is an endocrine hormone with broad metabolic actions at supraphysiological concentrations but unclear physiological function, related to endoplasmic reticulum (ER) stress. ER stress activates the unfolded protein response (UPR), a cellular repair mechanism that maintains cellular homeostasis during protein folding stress. Using proximity labeling, we assessed the intracellular action of FGF21 at its receptor β-klotho (KLB) and discovered associations with protein folding in the ER, ER stress, and H_2S production. We found that FGF21 increases enzymatic sulfide production and enhances, but does not initiate, the UPR. This FGF21 action is blunted by genetic or pharmacological inhibition of sulfide signaling and is phenocopied by an H_2S donor *in vivo*. FGF21 modulating the UPR requires KLB, and even physiological levels of FGF21 modulate the UPR via increased hepatic H_2S production. Collectively, we reveal a novel physiological role of FGF21 as an endocrine stress hormone that enhances the UPR via increased sulfide signaling.

INTRODUCTION

Fibroblast growth factor 21 (FGF21) was first described as a metabolic hormone that decreases body weight while improving glucose homeostasis in diet-induced obese (DIO) mice,[1] which spurred interest in exploring the pharmacological potential of FGF21 analogs for the control of systemic energy metabolism in humans. While FGF21 shows only minor effects on glucose control in humans, it clearly improves dyslipidemia and metabolic dysfunction-associated fatty liver disease (MAFLD).[1,2] Although the pharmacological potential of FGF21 has been verified in numerous studies,[3–6] the physiological role of FGF21 remains largely unknown. In rodents, FGF21 is secreted upon fasting[7] or after feeding on a ketogenic diet (KD),[8] but it is dispensable for the metabolic adaptation to fasting.[9] In humans, FGF21 is not increased following the consumption of a KD, and the plasma levels of FGF21 do not rise acutely in response to fasting.[10] Plasma levels of FGF21 also increase in response to dietary methionine[11] or protein restriction,[12,13] thus potentially indicating that FGF21 is an endocrine signal that governs systemic adaptation to a low-protein diet.[12,13] In both rodents and humans, the plasma levels of FGF21 increase upon ethanol intake,[14,15] and its expression increases with high-fat diet (HFD) feeding or excessive sugar intake.[16,17] More recently, FGF21 was identified as an endoplasmic reticulum (ER) stress hormone that is induced as part of the unfolded protein response

Please cite this article in press as: Grandl et al., FGF21 reduces ER stress by enhancing the unfolded protein and integrated stress responses through increased sulfide signaling, Cell Metabolism (2026), https://doi.org/10.1016/j.cmet.2026.05.011

(UPR).[18–20] The UPR is a broadly conserved signaling pathway initiated by the detection of misfolded proteins in the ER via the ER-membrane receptors *inositol-requiring enzyme 1 α* (IRE1α), *protein kinase R (PKR)-like endoplasmic reticulum kinase* (PERK), and *activating transcription factor 6* (ATF6), activating a wide range of signaling and transcriptional responses to restore cellular homeostasis.[21] The second branch of the UPR, commonly referred to as the integrated stress response (ISR), leads to the phosphorylation of *translation elongation initiation factor 2α* (eIF2α) and subsequent induction of *activating transcription factor 4* (ATF4) expression.[22] This branch of the UPR receives input from four different kinases, one of which is PERK, to collectively integrate the signals for protein folding, oxidative, and nutrition stress, and infection.[23] FGF21 is a direct transcriptional target of ATF4 during amino acid deprivation[18] or ER stress,[19] and of the IRE1α-mediator *spliced x-box binding protein 1* (XBP1s) due to ER stress.[20] The cognate receptor of FGF21, β-klotho (KLB), is upregulated in mouse liver in response to ER stress,[24] and FGF21 modulates exogenously induced ER stress.[25] FGF21 directly binds to KLB, which initiates heterodimerization of the FGF21-KLB complex with FGF-receptor 1 (FGFR1) and downstream phosphorylation of the MAP-kinase ERK1/2.[26,27] While the intracellular signaling mechanisms of FGF21-KLB are only poorly understood, additional downstream signals are assumed to include the activation (phosphorylation) of adenosine monophosphate kinase (AMPK), ribosomal protein s6 kinase (S6K), and mammalian target of rapamycin (mTOR).[28]

Insight into the physiology of sulfide signals (SSs) dates back to the observation that endogenous enzymatic H_2S production has a vasodilative effect.[29–31] Subsequently, H_2S was shown to signal via per- or polysulfidation of cysteine residues[32] generating sulfane sulfur,[33] which modifies the activity of a wide range of proteins and results in increased cell survival under various stresses.[34–36] Proteins with reported enzymatic H_2S or persulfide production[37] are cystathionine gamma lyase (CGL, gene name CTH), cystathionine beta synthase (CBS), 3-mercaptopyruvate sulfurtransferase (MPST),[34,35] and cysteinyl t-RNA synthase 2 (CARS2).[38]

Proximity labeling was recently established as a powerful tool to study transient protein-protein interactions.[39] Its basic principle is to stably biotinylate proteins in the proximity of a protein of interest, which can then be isolated and analyzed by mass-spectrometry-based proteomics.[39] Using proximity labeling, we here report the identification of novel FGF21-KLB interaction partners, most notably CBS. In a series of *in vitro* and *in vivo* studies, we show that FGF21-KLB acts via CBS or CGL under physiological and stimulated conditions to enhance the UPR via sulfide signaling, which we identified as a novel core second messenger of the UPR. In summary, we identify a novel and highly relevant physiological function of FGF21, in that it regulates the UPR via sulfide signaling.

RESULTS

Proximity labeling reveals the association of FGF21/KLB with protein folding, ER stress, and sulfide signaling

We used a proximity labeling strategy based on the engineered ascorbate peroxidase (APEX2)[39] to study FGF21 signaling by labeling the C-terminal (intracellular) end of KLB with APEX2 (KLB-APEX), thus enabling the enrichment and mass spectrometry analysis of interaction partners (Figure 1A). Constitutively expressing KLB-APEX in HEK293 cells (KLB-APEX cells) enabled biotin labeling that was dependent on biotin-phenol and H_2O_2, and the isolation of biotinylated proteins by streptavidin affinity purification (Figures 1B and 1C). The specificity of KLB-APEX labeling was confirmed by a comparison with ubiquitously expressed APEX2 in the absence of exogenous FGF21 (Figure S1A), which showed a clear difference in isolated biotin-labeled proteins by western blot (Figure S1B). Consistent with the cellular localization of KLB, Gene Ontology (GO)-term enrichment analysis revealed that most of the identified unstimulated KLB-linked proteins correspond to membrane-localized processes (Figure S1C). To identify FGF21-dependent KLB-APEX signaling interactions, we labeled KLB-APEX-interacting proteins at different time points after FGF21 treatment (Figure 1D). To capture the time-dependent kinetics of FGF21-induced phosphorylation of ERK (Figures 1E and 1F), we focused on time points between 0 and 8 min of FGF21 treatment. At the proteome level, the top FGF21-dependently enriched protein was cystathionine β-synthase (CBS), a key enzyme for H_2S production, which is implicated in various cellular stress responses, tissue injury, and apoptosis[36] (Figure 1G). This FGF21-enhanced association of KLB with CBS was confirmed in an independent experiment, and GO-term enrichment analysis of the FGF21-induced changes in APEX-labeled proteins revealed the enrichment of proteins associated with protein folding in the ER, the response to ER stress, and the response to oxidative stress among the top 10 enriched GO terms (Figure 1H). These data thus indicate an association of FGF21 with sulfide signaling and a role in protein folding and ER stress.

FGF21 action increases sulfide signaling and enhances the UPR and ISR

Investigating persulfide production using the sulfane sulfur probe SSP4, we found that overnight treatment with FGF21, or ER stress induced by tunicamycin (Tm), caused an increase of sulfide signaling in KLB-APEX cells, as indicated by elevated persulfides (Figure 2A). Although hepatic H_2S production was unchanged in mice after a single bolus administration of FGF21 (Figures S2A and S2B), we observed a significant increase in hepatic H_2S production after 14 days of daily subcutaneous (s.c.) FGF21 administration (Figures 2B and 2C). Importantly, this FGF21-induced increase of hepatic H_2S production was not due to increased CGL or CBS protein levels (Figures 2D and S2C). To unequivocally rule out indirect actions of FGF21 on the liver, we next tested the effect of FGF21 or Tm on hepatic persulfide production in *ex vivo* murine liver slices and found that both FGF21 and Tm increased SS production (Figure 2E). Intriguingly, exogenous FGF21 in FGF21KO (FGF21-knockout) liver slices produced a much larger increase of SSs, which suggests that endogenous FGF21 acts as a paracrine sulfide-inducing hormone in the liver (Figure 2F). Besides increasing hepatic H_2S production, daily FGF21 administration for 2 weeks caused an increase in eIF2α phosphorylation in lean animals (Figure 2D and 2G), which was also observed after a single day of treatment (Figures S2D and S2E). Counterintuitively, this led to a mild reduction in hepatic ATF4 protein levels (Figure 2H). Next, we examined both the direct effects of

Please cite this article in press as: Grandl et al., FGF21 reduces ER stress by enhancing the unfolded protein and integrated stress responses through increased sulfide signaling, Cell Metabolism (2026), https://doi.org/10.1016/j.cmet.2026.05.011

CellPress
OPEN ACCESS

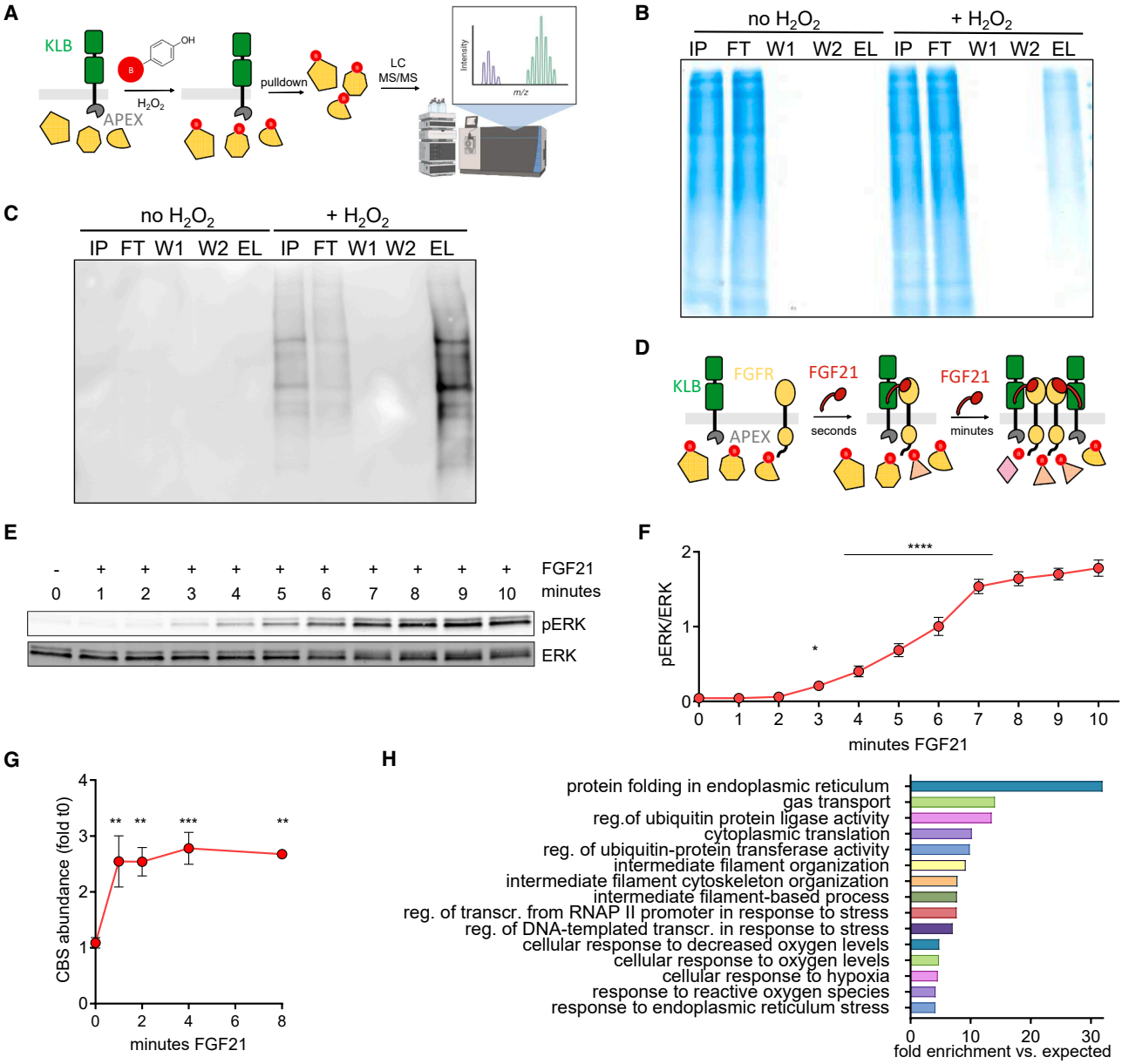

Figure 1. Proximity labeling reveals the association of FGF21/KLB with protein folding, ER stress, and sulfide signaling

(A) Scheme of the APEX2 labeling strategy. Expressing a KLB-APEX fusion protein allows biotinylation, selective isolation, and the measurement by LC-MS/MS of proteins near KLB.

(B) Coomassie staining of precipitated biotinylated proteins. IP, input; FT, flowthrough; W, wash; EL, eluate.

(C) Western blot of biotinylated proteins precipitated with streptavidin beads, detected with Strep-Tactin.

(D) Scheme of the strategy to elucidate FGF21 signaling by labeling proteins near KLB-FGF21 at different times of FGF21 treatment.

(E) Western blot of phospho-ERK (pERK) and total ERK after different times of FGF21 treatment.

(F) Quantification of the pERK/ERK western blot signal by densitometry. $n = 3$ independent experiments.

(G) Relative abundance of CBS protein labeled after FGF21 treatment. $n = 4$ independent experiments.

(H) Top GO-biological process terms in the FGF21-KLB interactome. reg., regulation.

Data are presented as mean ± SEM. Statistical analysis was done by one-way ANOVA, $^{**}p < 0.01$, $^{***}p < 0.005$, and $^{****}p < 0.001$.

See also Figure S1, Table S1, and Data S1.

FGF21 and the interaction with Tm-induced ER stress by comparing acute effects (4 h of treatment) and overnight pre-treatment of FGF21 followed by 4 h of Tm co-treatment or FGF21. Due to persistent basal activation of the ISR in KLB-APEX cells, we focused on the first branch of the UPR, measuring XBP1s protein (Figure 2I). While FGF21 alone caused only a minor transient increase in XBP1s protein (Figure 2J), it significantly enhanced Tm-induced XBP1s levels, an effect that

Please cite this article in press as: Grandl et al., FGF21 reduces ER stress by enhancing the unfolded protein and integrated stress responses through increased sulfide signaling, Cell Metabolism (2026), https://doi.org/10.1016/j.cmet.2026.05.011

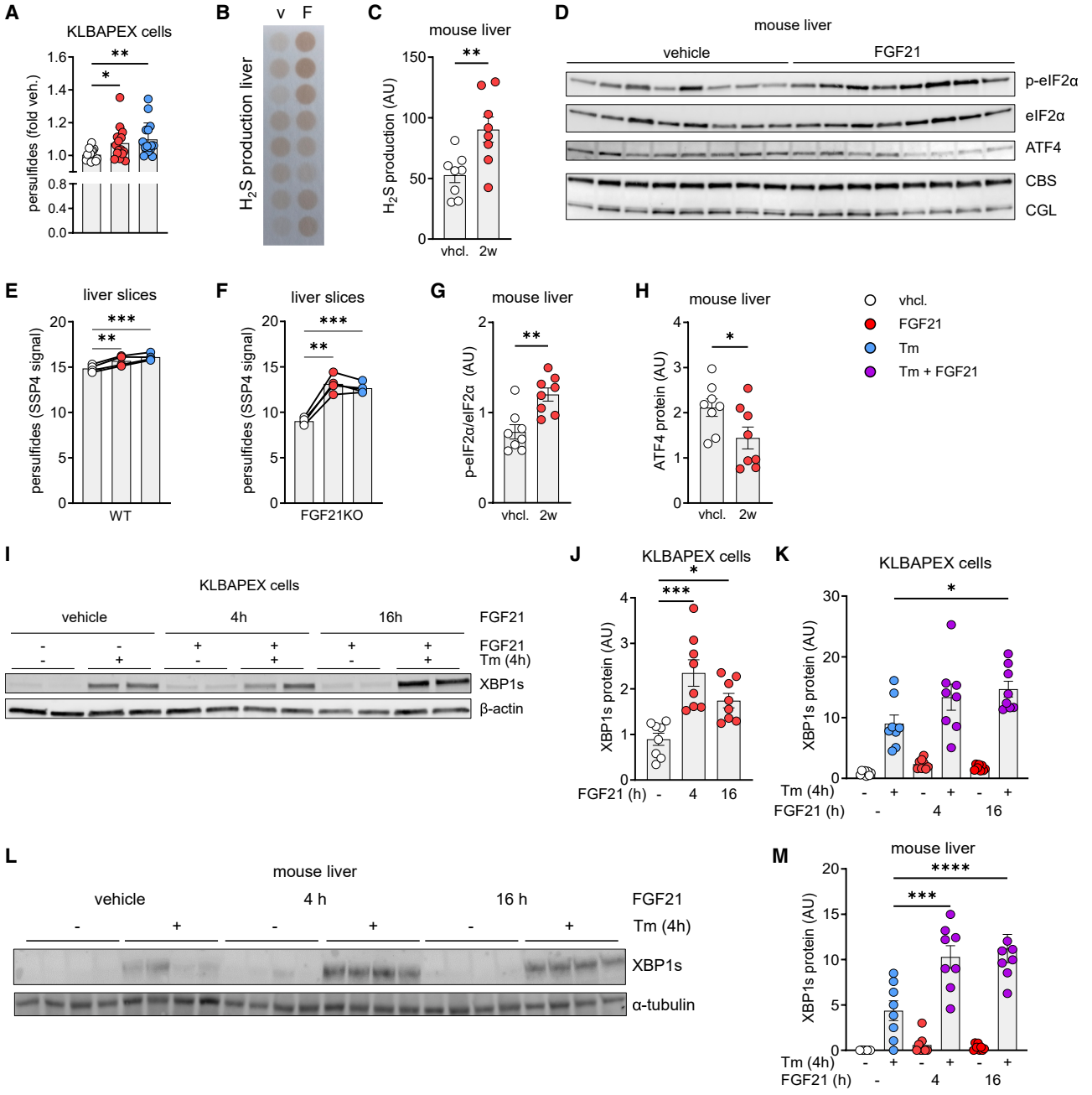

Figure 2. FGF21 action increases sulfide signaling and enhances the UPR and ISR

(A) Signal of the fluorescent sulfane sulfur probe SSP4 in KLB-APEX-expressing HEK cells (KLB-APEX), after overnight treatment with FGF21 or Tm, normalized to control. *n* = 16 independent experiments with 3 technical replicates.

(B) Lead acetate staining of H_2S produced in liver protein extracts from lean mice treated with vehicle (v) or FGF21 (F) for 2 weeks.

(C) Densitometric quantification of lead acetate staining from (B), arbitrary units (AU). *n* = 8 mice per group.

(D) Western blot of protein from livers of lean wild-type (WT) mice treated with FGF21 or vehicle for 2 weeks.

(E and F) Persulfide production measured by SSP4 in fresh liver slices from WT and FGF21KO mice, treated with vehicle, FGF21, or Tm. *n* = 4 mice per group.

(G and H) Densitometric quantification of p-eIF2α and ATF4 levels from western blots as in (D), arbitrary units (AU). *n* = 8 mice per group.

(I) Western blot of protein from KLB-APEX cells treated with FGF21 or vehicle for the indicated times, and Tm for 4 h.

(J) Densitometric quantification of XBP1s levels from western blots as in (I), subset without Tm, arbitrary units (AU). *n* = 8 independent experiments per group.

(K) Densitometric quantification of XBP1s levels from western blots as shown in (I), arbitrary units (AU), *n* = 8 independent experiments per group. *FGF21, ****Tm by two-way ANOVA.

(L) Western blot of protein from livers of WT mice treated with FGF21 or vehicle for the indicated times, and Tm for 4 h.

(legend continued on next page)

Please cite this article in press as: Grandl et al., FGF21 reduces ER stress by enhancing the unfolded protein and integrated stress responses through increased sulfide signaling, Cell Metabolism (2026), https://doi.org/10.1016/j.cmet.2026.05.011

was maximized by overnight pretreatment (Figure 2K). On the mRNA level, FGF21 caused a transient increase in Xbp1s expression (Figure S2F) and further enhanced Tm-induced Xbp1s levels (Figure S2G). Consistent with this, we found that the hepatic levels of XBP1s protein in response to Tm increased in mice after FGF21 administration (Figures 2L and 2M). Collectively, these data indicate that FGF21 action induces SSs and enhances but does not initiate the UPR and ISR.

FGF21's effects on the UPR require sulfide signaling and are mimicked by an H_2S donor

To determine whether FGF21 action on the UPR is mediated via sulfide production, we knocked down the key H_2S-producing enzymes CBS and CGL (gene name CTH) in KLB-APEX cells using small interfering RNA (siRNA) (Figure S3A). Reduced expression of both enzymes blunted the observed baseline effects of FGF21 on XBP1s expression, with a more pronounced effect of CBS knockdown (Figure S3B). Similarly, chemical inhibition of SSs using the broad pyridoxal-phosphate binding SS inhibitor aminooxoacetic acid (AOA)[40] (Figure 3A) confirmed that blocking SSs severely blunts both the basal effects of FGF21 alone (Figure 3B) and its modulation of ER stress (Figure 3C). Because CGL rather than CBS is the primary H_2S-producing enzyme in the liver,[41] we next assessed the hepatic interaction of KLB with CGL protein in mice treated with FGF21. *In situ* proximity ligation assays in liver cryosections confirmed FGF21-stimulated KLB-CGL interaction in FGF21KO mice (Figures 3D and 3E), an effect that was less pronounced in wild-type (WT) mice (Figures S3C and S3D), which again suggested the paracrine effects of endogenous FGF21. Experiments in *ex vivo* liver slices of CTH-knockout (CTHKO) C57BL/6 mice, which had no detectable liver CGL and drastically reduced hepatic H_2S production (Figures S3E–S3G), demonstrated that FGF21's ability to increase hepatic persulfide production requires CGL (Figure 3F), thus demonstrating functional interaction in mouse liver. As expected, we also confirmed that reducing SSs genetically blunted the action of FGF21 on the UPR *in vivo* (Figures 3G and 3H). Furthermore, both FGF21 treatment and the loss of CGL caused a mild activation of the ISR in the absence of exogenous ER stress (Figures 3I and S3H). In a gain-of-function experiment using the H_2S donor GYY4137 (Figure 3J), we found that H_2S mimicked FGF21's action on the UPR, enhancing XBP1s protein induction due to ER stress (Figure 3K), and mildly inducing the ISR alone (Figure 3L). As in our acute studies with FGF21, we did not detect elevated H_2S production in the livers of GYY4137-treated animals (Figures S3I and S3J), despite observing the H_2S action on the UPR. These data indicate that the action of FGF21 on the UPR requires SSs, and exogenous sulfide mimics FGF21 action on the UPR.

Pharmacological and physiological levels of FGF21 regulate ER stress and H_2S production

In DIO mice, which represent a more physiological form of ER stress than induction via Tm, 2 weeks of daily s.c. administration of FGF21 produced a similar increase in liver H_2S production as in lean mice (Figures 4A and 4B), but unlike in lean mice, it also slightly increased hepatic CGL levels (Figures 4C and 4D). Unexpectedly, FGF21 did not increase hepatic eIF2α phosphorylation (Figures 4C and 4E) in DIO mice but did reduce hepatic ATF4 expression as in lean mice (Figures 4C, 4F, and 4G). Moreover, Xbp1s mRNA (Figure S4A) was reduced, and there was a trend toward reduced *DNA damage-inducible transcript 3* (Ddit3) mRNA (Figure S4B). Assessing the effect of physiological levels of endogenous FGF21 in DIO mice via global deletion of FGF21 in C57BL/6 mice (FGF21KO), we found a robust increase in plasma FGF21 levels in WT mice but no detectable levels in FGF21KO mice after 6 months of HFD feeding (Figure 4H). DIO mice exhibited a significant decline in liver H_2S production independent of genotype (Figures 4I and 4J), which was driven by a strong reduction in liver CGL protein levels (Figures 4K and 4L). Levels of the known CGL transcription factor ATF4 were solidly reduced in the livers of DIO mice (Figure 4K), which was unexpected since the upstream eIF2α phosphorylation was increased. However, consistent with the shown pharmacological effects, liver extracts from lean WT mice with preserved physiological levels of FGF21 showed higher hepatic H_2S production than FGF21KO liver extracts (Figures 4I and 4J), without increased CGL levels (Figures 4K and 4L). The lack of physiologic FGF21 also led to slight elevations of hepatic ER stress, as evidenced by increased eIF2α phosphorylation in lean mice (Figures 4K and 4M), whereas DIO caused a strong increase in p-eIF2α independent of genotype (Figures 4K and 4N). At the level of downstream ATF4 protein, we observe no difference in lean mice (Figures 4K and 4O) but a significant increase in KO DIO mice (Figures 4K and 4P), albeit at the reduced ATF4 levels that we observe in DIO. The metabolic benefits of physiological FGF21 in DIO mirrored the observed effects on sulfide production and ER stress, with the FGF21KO displaying a more severe impairment in glucose tolerance (Figures S4C and S4D) and insulin sensitivity (Figures S4E and S4F). These data indicate a protective role of physiological levels of FGF21 for liver ER stress and H_2S production.

FGF21's effects on the UPR and H_2S production require KLB

Comparing KLB-deficient HEK293 cells to KLB-APEX cells revealed that the effects of FGF21 on the UPR require KLB expression (Figure 5A). The presence of the receptor was necessary for both FGF21's activation of canonical ERK1/2 (Figure 5B), as well as enhanced XBP1s protein levels by FGF21 alone (Figure 5C) or with exogenously induced ER stress (Figure 5D). The overexpression of KLB also increased basal XBP1s levels but reduced stress-induced levels compared with HEK293 cells (Figures 5C and 5D). Surprisingly, we observed that Tm-induced ER stress reduced KLB protein levels, expressed under the CMV promoter, whereas FGF21 drastically increased them, and the combination of the two resulted in KLB expression comparable to that of untreated cells (Figure 5E). This indicates that FGF21 protected the

(M) Densitometric quantification of XBP1s levels from western blots as in (L), arbitrary units (AU). $n = 8$ mice per group. ***FGF21, ****Tm by two-way ANOVA. vhcl and v, vehicle; F, FGF21; Tm, tunicamycin.

Data are presented as mean ± SEM. Statistical analysis was done by one- or two-way ANOVA with post hoc comparison as appropriate. $^{*}p < 0.05$, $^{**}p < 0.01$, $^{***}p < 0.005$, and $^{****}p < 0.001$.

See also Figure S2 and Data S1.

Please cite this article in press as: Grandl et al., FGF21 reduces ER stress by enhancing the unfolded protein and integrated stress responses through increased sulfide signaling, Cell Metabolism (2026), https://doi.org/10.1016/j.cmet.2026.05.011

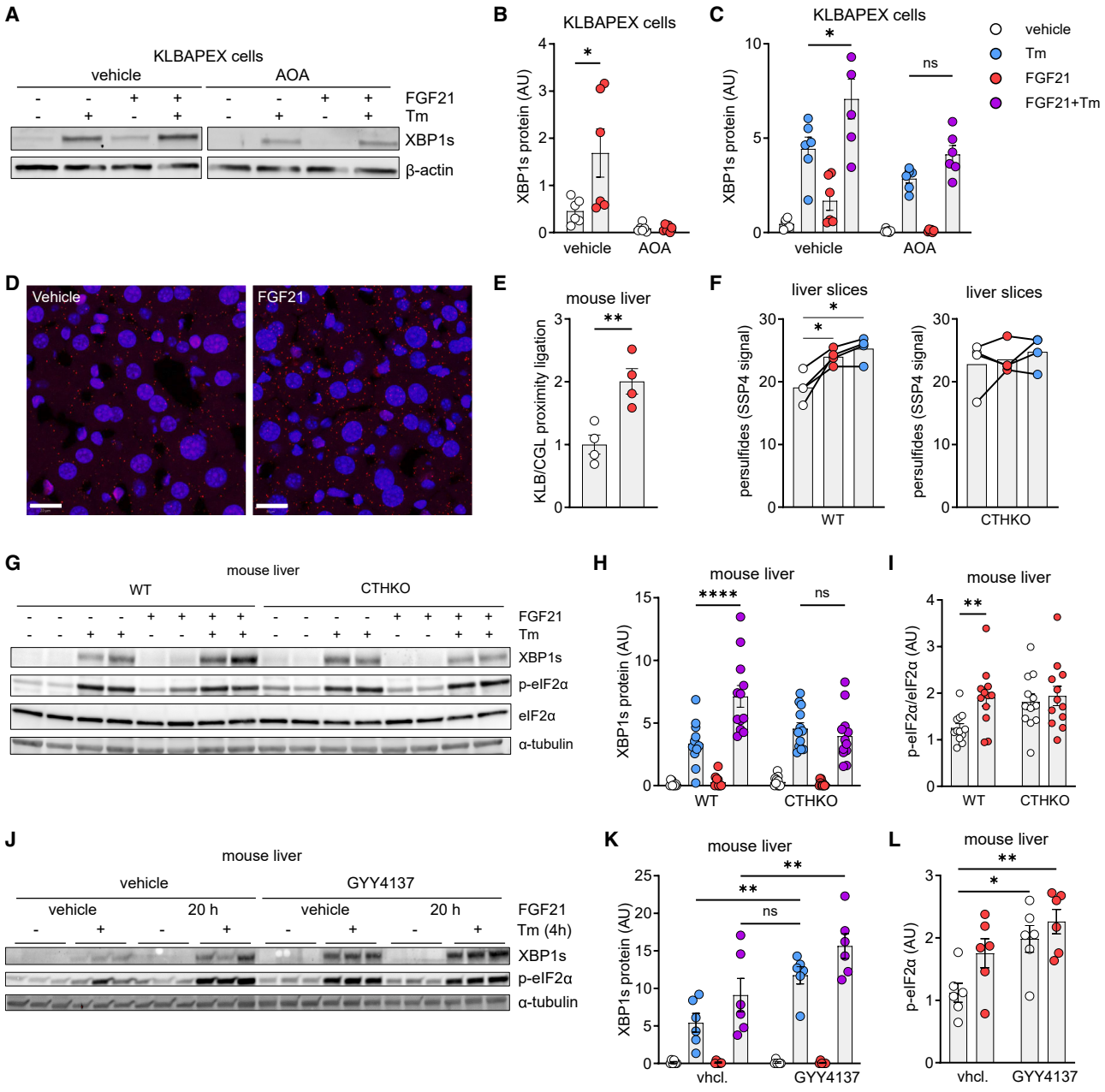

Figure 3. FGF21's effects on the UPR require sulfide signaling and are mimicked by an H_2S donor

(A) Western blot of protein from KLB-APEX cells, treated with the broad H_2S-production inhibitor AOA, FGF21, Tm, or vehicle for 4 h.

(B) Densitometric quantifications of XBP1s protein levels from western blots as shown in (A), subset without Tm, arbitrary units (AU). *n* = 6 independent experiments.

(C) Densitometric quantifications of XBP1s protein levels from western blots as shown in (A), arbitrary units (AU). *n* = 6 independent experiments.

(D) Representative images of proximity ligation assays (PLA) between KLB and CGL performed in liver cryosections of FGF21KO mice treated with vehicle or FGF21, nuclei stained with DAPI (blue) and proximity ligation signal with Texas Red (red). Scale bar, 20 μm.

(E) Quantification of PLA signal and fold change. *n* = 4 mice per group.

(F) Persulfide production in fresh liver slices from WT and CTHKO mice treated with vehicle, FGF21, or Tm, measured by SSP4. *n* = 4 mice per group.

(G) Western blot of protein from livers of WT or CTHKO mice treated with FGF21 for 16 h and Tm for 4 h.

(H) Densitometric quantifications of XBP1s protein levels from blots as shown in (G), arbitrary units (AU). *n* = 12 mice per group.

(I) Densitometric quantifications of p-eIF2α protein levels from blots as shown in (G), subset without Tm, arbitrary units (AU). *n* = 12 mice per group.

(J) Western blot of protein from livers of WT mice treated with vehicle or the H_2S donor GYY4137 and FGF21 for 20 h, and Tm for 4 h.

(K) Densitometric quantifications of XBP1s protein levels from western blots as shown in (J), arbitrary units (AU). *n* = 6 mice per group.

(legend continued on next page)

Please cite this article in press as: Grandl et al., FGF21 reduces ER stress by enhancing the unfolded protein and integrated stress responses through increased sulfide signaling, Cell Metabolism (2026), https://doi.org/10.1016/j.cmet.2026.05.011

cells from the negative effects of the ER stress on protein synthesis. Next, we knocked out KLB in the liver with an adeno-associated virus expressing Cre-recombinase under the thyroid hormone-binding globulin promoter (KLBKO) or eGFP (WT), in mice carrying a homozygous floxed KLB allele (Figure S5A). Daily s.c. FGF21 administration for 2 weeks did not cause an increase in hepatic H_2S production in either WT or KLBKO mice, but the KO mice had significantly increased hepatic H_2S production (Figures 5F and 5G) without changes in CBS or CGL protein levels (Figures 5I and S5B), and they had elevated hepatic FGF21 mRNA (Figure 5H). Consistent with this, KLBKO mice displayed markedly increased hepatic ISR activation compared to WT controls (Figures 5I and 5J), and this response was abolished in the absence of hepatic KLB (Figure 5K). ATF4 protein levels were not significantly changed between genotypes (Figure S5C). These findings suggest that KLB deficiency promotes ER stress and the ISR, leading to a compensatory increase in FGF21 and H_2S production, while confirming that KLB is required for FGF21's effects on the UPR.

DISCUSSION

Employing a discovery-driven dynamic proximity labeling strategy to map the intracellular KLB interactome, we reveal a novel function of FGF21 as a hormonal enhancer of the UPR and ISR, which acts via increased enzymatic sulfide production. ER stress and metabolic impairments are functionally and causally interconnected,[42,43] and our data indicate that the metabolic benefits of FGF21 are part of a hormonal response to stress.

While FGF21 is canonically induced downstream of the UPR during cellular stress,[18–20] our findings demonstrate that FGF21 actively feeds back to enhance the UPR. Crucially, the activation of the UPR and ISR must be distinguished from the actual chemical or physical stress. We observed that while FGF21 elicits a moderate transient increase in UPR readouts in healthy systems (Figures 2 and 3), it lowers these markers in chronically stressed systems (Figure 4). This indicates that rather than initiating the UPR, FGF21 potentiates this pathway in the presence of stressors, thus sensitizing the cell to boost the adaptive response and protein folding capacity. The changes in overexpressed KLB protein in KLB-APEX cells, where FGF21 increases basal KLB levels and prevents their reduction during ER stress (Figure 5), illustrate this particularly well.

Mechanistically, we show that FGF21 enhances the UPR via the increased enzymatic production of SSs (Figure 3). Importantly, our data also show that the induction of ER stress itself increases enzymatic SS production in the presence or absence of FGF21 (Figures 2 and 3), which indicates that SSs are part of a positive feedback loop within the UPR independently of FGF21. This aligns with prior evidence that H_2S sustains eIF2α phosphorylation by inhibiting the phosphatases PTP1b[44] and PP1c[45] via persulfidation. By orthogonally driving SSs, FGF21 inhibits the phosphatases that turn off the UPR, preventing the premature deactivation of the stress response. This positive feedback loop reveals that UPR/ISR activation is not merely a passive readout of stress but integrates endogenous stress signals and FGF21's hormonal action.

The mechanism of FGF21 we describe—potentiating the response to misfolded proteins without directly triggering the costly UPR in the absence of stress—represents an elegant strategy for an endocrine hormone of protein folding stress. It also offers a molecular rationale for previous observations that FGF21 enhances exocrine pancreatic function[46] and mitigates chemically induced ER stress.[25]

The data in mice with severely reduced hepatic KLB levels corroborate our findings that SSs are a core positive feedback loop of the UPR modulated by FGF21/KLB signaling. We observed that the loss of hepatic KLB causes increased stress, which leads to compensatory FGF21 upregulation and increased ISR activation and sulfide production (Figure 5F).

Since both ATF4 and its transcriptional target CGL have been reported to increase during ER stress,[47] it was surprising to see their hepatic protein levels decrease drastically in DIO mice (Figure 4). This suggests that high activity of ATF4 in fatty liver might have negative consequences causing its endogenous reduction, which is consistent with recent reports demonstrating that the ablation of ATF4 can reduce hepatic fibrosis.[48,49] Chronic FGF21 action always led to reduced hepatic ATF4 (Figures 2 and 4), irrespective of its diet-dependent hepatic levels, and unexpectedly did not mirror hepatic eIF2α phosphorylation, which is upstream of ATF4. This surprising uncoupling between eIF2α phosphorylation and ATF4 levels probably reflects the different timescales of these signals, where eIF2α phosphorylation responds acutely, whereas ATF4 protein levels likely reflect a longer-term integration of signals. FGF21's effects on ATF4 are therefore consistent with FGF21 reducing chronic ER stress through increased UPR-responsiveness. Moreover, in lean mice, both the physiological and pharmacological levels of FGF21 increased hepatic H_2S production without increasing CGL protein (Figures 2 and 4), which points to FGF21-induced increased enzymatic CGL activity.

The physiological relevance of this signaling axis is underscored by the convergence of phenotypes associated with both FGF21 and H_2S. Both are implicated in the benefits of caloric restriction (CR), longevity, and stress resistance. For instance, the transsulfuration pathway is rewired during ER stress to favor H_2S production,[50] and H_2S orchestrates some of the metabolic adaptations to ER stress.[51] Activation of the ISR upregulates CGL,[47] as does induction of the mitochondrial UPR, inducing FGF21 together with CGL.[52] Increased H_2S production is essential for the metabolic benefits of CR,[53] and FGF21-overexpressing mice increase hepatic H_2S production[54] and exhibit increased lifespan,[55] as do DIO mice secreting overexpressed FGF21 from adipose tissue.[56] Moreover, FGF21 was demonstrated to reverse MASH acting directly on the liver and CNS,[57] which is in line with the direct hepatic FGF21 effects we report. Lastly, protein persulfidation was linked to aging in mice,[58] and dietary supplementation of sulfides increased the life and healthspan in male mice.[59] Our data provide the missing

(L) Subset of the data in (K) without Tm, arbitrary units (AU). $n = 6$ mice per group. vhcl, vehicle; Tm, tunicamycin; AOA, aminooxyacetic acid.
Data are presented as mean ± SEM. Statistical analysis was done by two- or three-way ANOVA with post hoc comparison as appropriate. $^{*}p < 0.05$, $^{**}p < 0.01$, and $^{****}p < 0.001$.
See also Figure S3 and Data S1.

Please cite this article in press as: Grandl et al., FGF21 reduces ER stress by enhancing the unfolded protein and integrated stress responses through increased sulfide signaling, Cell Metabolism (2026), https://doi.org/10.1016/j.cmet.2026.05.011

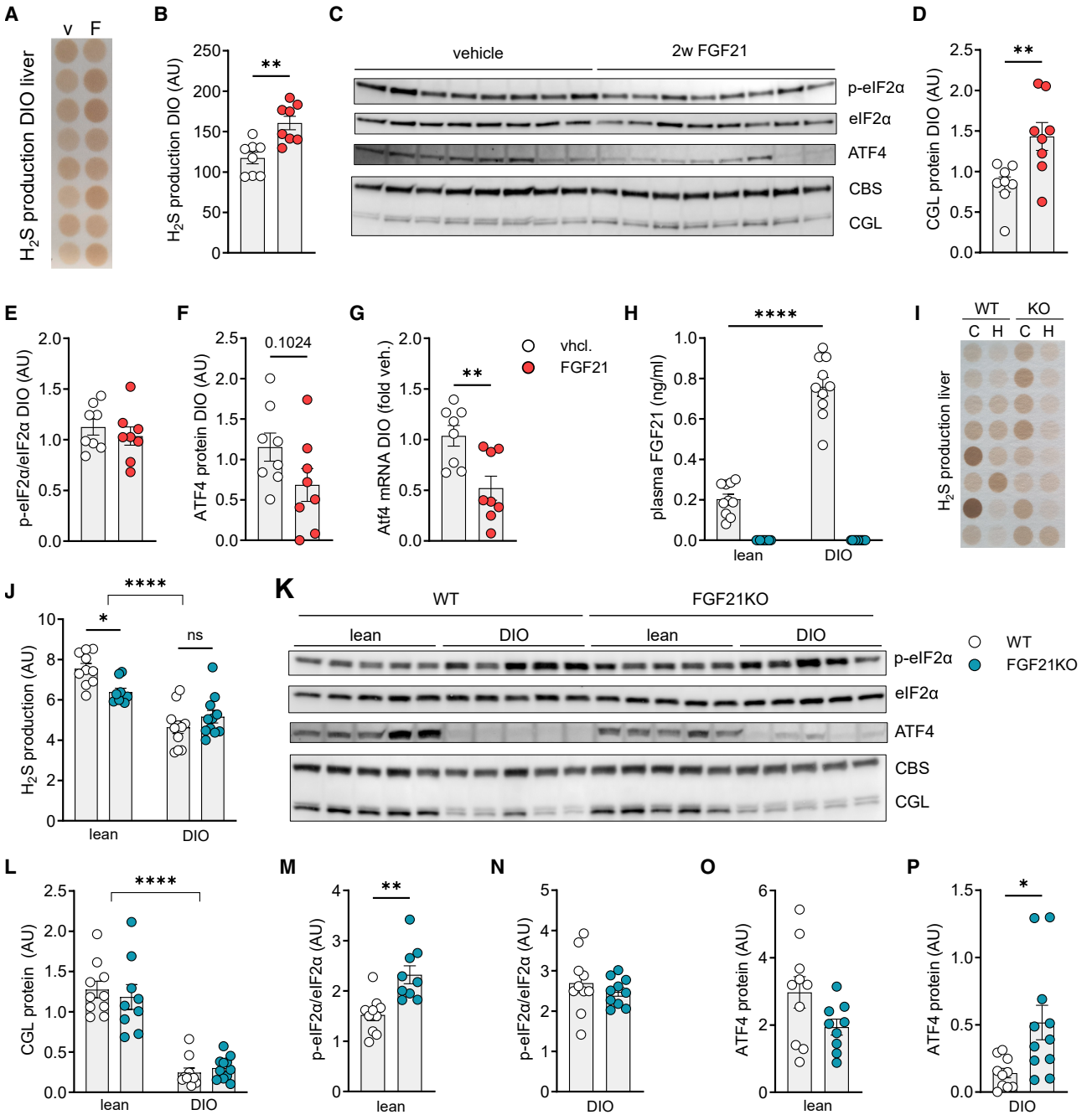

Figure 4. Pharmacological and physiological levels of FGF21 regulate ER stress and H_2S production

(A) Lead acetate staining of H_2S produced in liver protein extracts from DIO WT mice treated with vehicle (v) or FGF21 (F) for 2 weeks.

(B) Densitometric quantifications of lead acetate staining from (A), arbitrary units (AU). *n* = 8 mice per group.

(C) Western blot of protein from livers of DIO WT mice treated with FGF21 or vehicle for 2 weeks.

(D–F) Densitometric quantifications of CGL, p-eIF2α, and ATF4 levels from western blots as shown in (C), arbitrary units (AU). *n* = 8 mice per group.

(G) Relative Atf4 mRNA levels from liver of DIO mice treated with vehicle or FGF21 for 2 weeks. *n* = 8 mice per group.

(H) Plasma FGF21 protein levels from WT or FGF21KO mice after 33 weeks of chow or HFD feeding. *n* = 10 lean WT; *n* = 9 lean KO; *n* = 10 DIO WT; *n* = 11 DIO KO mice.

(I) Lead acetate staining of H_2S produced in liver protein extracts from WT or FGF21KO mice fed with chow (C) or HFD (H) for 33 weeks.

(J) Densitometric quantifications of lead acetate staining as shown in (G), arbitrary units (AU). *n* = 10 lean WT; *n* = 9 lean KO; *n* = 11 DIO WT; *n* = 11 DIO KO mice.

(K) Western blot of liver protein from WT or FGF21KO mice fed with chow or HFD for 33 weeks.

(legend continued on next page)

link between these various observations: FGF21 acts as an endocrine driver of cytoprotective sulfide signaling, eliciting broad benefits and increasing lifespan.

In summary, we propose that FGF21 functions fundamentally as an endocrine hormone of protein folding- and cellular stress. By inducing sulfide signaling to enhance the UPR, FGF21 enhances the cellular capacity to handle stress. This discovery redefines SSs as a core second messenger of the UPR and ISR and highlights the therapeutic potential of targeting the FGF21-sulfide axis for metabolic and age-related diseases.

Limitations of the study

We acknowledge limitations in quantifying the transient nature of sulfide signaling. The detection threshold for H_2S production in tissue extracts is high relative to likely physiologically active changes. Consequently, while chronic FGF21 treatment yielded robust differences in lean and DIO mice, acute treatment or the slow-release donor GYY4137 did not show detectable changes in bulk H_2S assays, despite functional efficacy. We addressed this by utilizing fresh liver slices to demonstrate acute persulfide production. Additionally, the tissue-specific distribution of H_2S-generating enzymes presents a variable. CBS is dominant in the brain and was identified in our HEK-cell proximity labeling approach, contributing more to effects in HEK cells. However, the liver relies more heavily on CGL, and after confirming KLB's interaction with CGL in mouse liver, we utilized CGL-deficient mice to validate our findings in the liver context due to the lethality of homozygous CBS deletion. Future studies will be required to dissect the tissue-specific contributions of these enzymes to FGF21 signaling, and the exact nature of how FGF21/KLB interacts with these enzymes to increase sulfide production.

RESOURCE AVAILABILITY

Lead contact

Further information and requests for resources and reagents should be directed to and will be fulfilled by the lead contact, Timo D. Müller (timodirk.mueller@helmholtz-munich.de).

Materials availability

This study did not generate any new, unique reagents.

Data and code availability

- Unprocessed source data underlying the display items in the manuscript are available in Data S1.
- The mass spectrometry proteomics data have been deposited in the ProteomeXchange Consortium via the PRIDE[60] partner repository with the dataset identifier PRIDE: PXD056693.

ACKNOWLEDGMENTS

We thank Peggy Dörfelt, Marlene Killian, Xenia Leonhardt, Wenjie Liu, Lara Fetzer, Laura Sehrer, and Emilija Malogajski from the IDO at Helmholtz Munich for their skillful technical assistance. Special thanks to Sebastian Müller from Biognosys for helpful discussions. G.G. received funding from the Swiss National Science Foundation (no. 178500). T.D.M. received funding for this work from the European Research Council ERC-CoG Trusted no. 101044445. The views and opinions expressed are, however, those of the authors only and do not necessarily reflect those of the European Union or the European Research Council. Neither the European Union nor the awarding authority can be held responsible for them. T.D.M. received funding from the German Research Foundation (DFG TRR296, TRR152, SFB1123, and GRK 2816/1) and the German Center for Diabetes Research (DZD e.V.). The graphical abstract was generated in Biorender.

AUTHOR CONTRIBUTIONS

G.G. conceptualized and initiated the project, designed and performed the experiments, analyzed and interpreted the results, and wrote the manuscript. A.-C.K., F.M., A.L., T.H., S.N., A.N., N.A.-R., M.A.R., A.K., Q.Z., and G.C. performed or assisted with the experiments, analyzed the results, and reviewed the manuscript. A.L. assisted in writing the manuscript. B.F., J.D., and A.C.-S. provided reagents or essential mouse lines (A.C.-S.) and reviewed the manuscript. K.H., S.M.H., and M.H.T. supervised experiments and reviewed the manuscript. T.D.M. supervised the experiments, analyzed and interpreted the results, and wrote the manuscript.

DECLARATION OF INTERESTS

M.H.T. is a member of the scientific advisory board of ERX Pharmaceuticals, Cambridge, MA. He was a member of the Research Cluster Advisory Panel (ReCAP) of the Novo Nordisk Foundation between 2017 and 2019. He attended a scientific advisory board meeting of the Novo Nordisk Foundation Center for Basic Metabolic Research, University of Copenhagen, in 2016. He received funding for his research projects from Novo Nordisk (2016–2020) and Sanofi-Aventis (2012–2019). He was a consultant for Bionorica SE (2013–2017), Menarini Ricerche S.p.A. (2016), and Bayer Pharma AG Berlin (2016). As the former Director of the Helmholtz Diabetes Center and the Institute for Diabetes and Obesity at Helmholtz Zentrum München (2011–2018), and since 2018, as the CEO of Helmholtz Zentrum München, he has been responsible for collaborations with a multitude of companies and institutions, worldwide. In this capacity, he discussed potential projects with and has signed/signs contracts for his institute(s) and for the staff for research funding and/or collaborations with industry and academia, worldwide, including but not limited to pharmaceutical corporations like Boehringer Ingelheim, Eli Lilly, Novo Nordisk, MediGene, Arbormed, BioSyngen, and others. In this role, he was/is further responsible for commercial technology transfer activities of his institute(s), including diabetes-related patent portfolios of Helmholtz Zentrum München, such as WO/2016/188932 A2 or WO/2017/194499 A1. M.H.T. confirms that, to the best of his knowledge, none of the above funding sources were involved in the preparation of this paper. T.D.M. receives research funding from Novo Nordisk and has received speaking fees from Eli Lilly, AstraZeneca, Novo Nordisk, and Merck. B.F. and J.D.D. were employees of Novo Nordisk while this work was performed. J.D.D. receives research funding from Eli Lilly and is a founder and shareholder in Volari Therapeutics, both of which are unrelated to this work.

DECLARATION OF GENERATIVE AI AND AI-ASSISTED TECHNOLOGIES IN THE WRITING PROCESS

During the preparation of this work, the authors used ChatGPT and Gemini in order to improve readability/conciseness of the text. After using this tool/service, the authors reviewed and edited the content as needed and take full responsibility for the content of the publication.

(L–P) Densitometric quantifications of CGL, p-eIF2α, and ATF4 levels from western blots as shown in (K), arbitrary units (AU). (L, M, and O) $n = 10$ lean WT; $n = 9$ lean KO; $n = 10$ DIO WT; $n = 11$ DIO KO mice. (N) $n = 10$ DIO mice per group. (P) $n = 10$ WT; $n = 11$ KO DIO mice. vhcl and v, vehicle; F, FGF21; HFD, high-fat diet; DIO, diet-induced obesity; C, chow; H, HFD.

Data are presented as mean ± SEM. Statistical analysis was done by pairwise *t* tests or two-way ANOVA with post hoc comparison as appropriate. $^{*}p < 0.05$, $^{**}p < 0.01$, and $^{****}p < 0.001$.

See also Figure S4 and Data S1.

Please cite this article in press as: Grandl et al., FGF21 reduces ER stress by enhancing the unfolded protein and integrated stress responses through increased sulfide signaling, Cell Metabolism (2026), https://doi.org/10.1016/j.cmet.2026.05.011

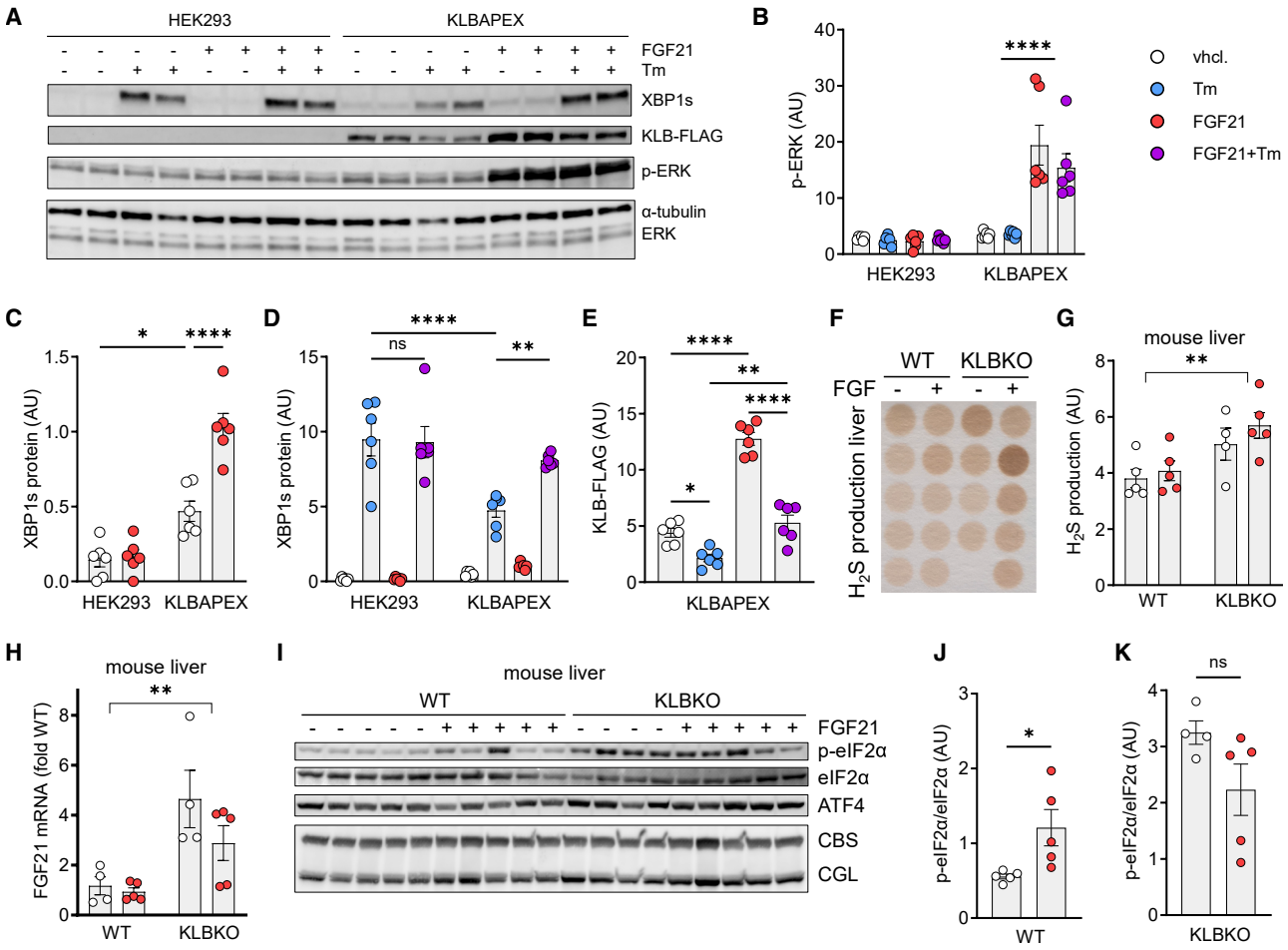

Figure 5. FGF21's effects on the UPR and H_2S production require KLB

(A) Western blot of protein from HEK293 or KLB-APEX cells treated with vehicle, FGF21, or Tm for 4 h.

(B and D) Densitometric quantifications of pERK and XBP1s protein levels from western blots as shown in (A), arbitrary units (AU). $n = 6$ independent experiments.

(C) Subset of (D) without Tm, arbitrary units (AU). $n = 6$ independent experiments.

(E) Densitometric quantifications of KLB-FLAG protein levels from western blots as shown in (B), arbitrary units (AU). $n = 6$ independent experiments.

(F) Lead acetate staining of H_2S produced in liver protein extracts from WT or KLBKO mice treated with vehicle or FGF21 for 2 weeks.

(G) Densitometric quantifications of lead acetate staining from (F), arbitrary units (AU). $n = 4$ mice for KO and vehicle; $n = 5$ mice for every other group.

(H) Relative FGF21 mRNA levels from liver of WT or KLBKO mice treated with vehicle or FGF21 for 2 weeks. $n = 4$ mice vehicle; $n = 5$ mice FGF21.

(I) Western blot from liver of WT or KLBKO mice treated with vehicle or FGF21 for 2 weeks.

(J and K) Densitometric quantifications of p-eIF2α levels from western blots as shown in (I), arbitrary units (AU). $n = 5$ mice per group WT; $n = 4$ mice for KO and vehicle; $n = 5$ mice for KO and FGF21. vhcl, vehicle; Tm, tunicamycin; KLBKO, klotho-beta knockout.

Data are presented as mean ± SEM. Statistical analysis was done by pairwise *t* tests or two-way ANOVA with post hoc comparison as appropriate. $^{*}p < 0.05$, $^{**}p < 0.01$, and $^{****}p < 0.001$.

See also Figure S5 and Data S1.

STAR★METHODS

Detailed methods are provided in the online version of this paper and include the following:

- KEY RESOURCES TABLE
- EXPERIMENTAL MODEL AND STUDY PARTICIPANT DETAILS
  - Animals and housing conditions
  - Cell culture
- METHOD DETAILS
  - APEX2 labelling and biotin pulldown
  - Filter aided sample preparation (FASP) digest
  - LC-MSMS measurements
  - Protein identification and label-free quantification
  - Western blot
  - H_2S-production measurements from liver extracts
  - Persulfide quantification in fresh liver slices
  - Proximity ligation assay
  - Gene expression analysis
- QUANTIFICATION AND STATISTICAL ANALYSIS

SUPPLEMENTAL INFORMATION

Supplemental information can be found online at https://doi.org/10.1016/j.cmet.2026.05.011.

Received: December 5, 2024
Revised: February 14, 2026
Accepted: May 26, 2026

REFERENCES

1. Geng, L., Lam, K.S.L., and Xu, A. (2020). The therapeutic potential of FGF21 in metabolic diseases: from bench to clinic. Nat. Rev. Endocrinol. *16*, 654–667. https://doi.org/10.1038/s41574-020-0386-0.
2. Chui, Z.S.W., Shen, Q., and Xu, A. (2024). Current status and future perspectives of FGF21 analogues in clinical trials. Trends Endocrinol. Metab. *35*, 371–384. https://doi.org/10.1016/j.tem.2024.02.001.
3. Coskun, T., Bina, H.A., Schneider, M.A., Dunbar, J.D., Hu, C.C., Chen, Y., Moller, D.E., and Kharitonenkov, A. (2008). Fibroblast growth factor 21 corrects obesity in mice. Endocrinology *149*, 6018–6027. https://doi.org/10.1210/en.2008-0816.
4. Holland, W.L., Adams, A.C., Brozinick, J.T., Bui, H.H., Miyauchi, Y., Kusminski, C.M., Bauer, S.M., Wade, M., Singhal, E., Cheng, C.C., et al. (2013). An FGF21-adiponectin-ceramide axis controls energy expenditure and insulin action in mice. Cell Metab. *17*, 790–797. https://doi.org/10.1016/j.cmet.2013.03.019.
5. Emanuelli, B., Vienberg, S.G., Smyth, G., Cheng, C., Stanford, K.I., Arumugam, M., Michael, M.D., Adams, A.C., Kharitonenkov, A., and Kahn, C.R. (2014). Interplay between FGF21 and insulin action in the liver regulates metabolism. J. Clin. Investig. *124*, 515–527. https://doi.org/10.1172/jci67353.
6. Fisher, F.M., and Maratos-Flier, E. (2016). Understanding the physiology of FGF21. Annu. Rev. Physiol. *78*, 223–241. https://doi.org/10.1146/annurev-physiol-021115-105339.
7. Inagaki, T., Dutchak, P., Zhao, G., Ding, X., Gautron, L., Parameswara, V., Li, Y., Goetz, R., Mohammadi, M., Esser, V., et al. (2007). Endocrine regulation of the fasting response by PPARalpha-mediated induction of fibroblast growth factor 21. Cell Metab. *5*, 415–425. https://doi.org/10.1016/j.cmet.2007.05.003.
8. Badman, M.K., Pissios, P., Kennedy, A.R., Koukos, G., Flier, J.S., and Maratos-Flier, E. (2007). Hepatic fibroblast growth factor 21 is regulated by PPARalpha and is a key mediator of hepatic lipid metabolism in ketotic states. Cell Metab. *5*, 426–437. https://doi.org/10.1016/j.cmet.2007.05.002.
9. Antonellis, P.J., Hayes, M.P., and Adams, A.C. (2016). Fibroblast growth factor 21-null mice do not exhibit an impaired response to fasting. Front. Endocrinol. (Lausanne) *7*, 77. https://doi.org/10.3389/fendo.2016.00077.
10. Fazeli, P.K., Lun, M., Kim, S.M., Bredella, M.A., Wright, S., Zhang, Y., Lee, H., Catana, C., Klibanski, A., Patwari, P., et al. (2015). FGF21 and the late adaptive response to starvation in humans. J. Clin. Investig. *125*, 4601–4611. https://doi.org/10.1172/jci83349.
11. Stone, K.P., Wanders, D., Orgeron, M., Cortez, C.C., and Gettys, T.W. (2014). Mechanisms of increased in vivo insulin sensitivity by dietary methionine restriction in mice. Diabetes *63*, 3721–3733. https://doi.org/10.2337/db14-0464.
12. Laeger, T., Henagan, T.M., Albarado, D.C., Redman, L.M., Bray, G.A., Noland, R.C., Münzberg, H., Hutson, S.M., Gettys, T.W., Schwartz, M.W., et al. (2014). FGF21 is an endocrine signal of protein restriction. J. Clin. Investig. *124*, 3913–3922. https://doi.org/10.1172/jci74915.
13. Laeger, T., Albarado, D.C., Burke, S.J., Trosclair, L., Hedgepeth, J.W., Berthoud, H.R., Gettys, T.W., Collier, J.J., Münzberg, H., and Morrison, C.D. (2016). Metabolic responses to dietary protein restriction require an increase in FGF21 that is delayed by the absence of GCN2. Cell Rep. *16*, 707–716. https://doi.org/10.1016/j.celrep.2016.06.044.
14. Song, P., Zechner, C., Hernandez, G., Cánovas, J., Xie, Y., Sondhi, V., Wagner, M., Stadlbauer, V., Horvath, A., Leber, B., et al. (2018). The hormone FGF21 stimulates water drinking in response to ketogenic diet and alcohol. Cell Metab. *27*, 1338–1347.e4. https://doi.org/10.1016/j.cmet.2018.04.001.
15. Choi, M., Schneeberger, M., Fan, W., Bugde, A., Gautron, L., Vale, K., Hammer, R.E., Zhang, Y., Friedman, J.M., Mangelsdorf, D.J., et al. (2023). FGF21 counteracts alcohol intoxication by activating the noradrenergic nervous system. Cell Metab. *35*, 429–437.e5. https://doi.org/10.1016/j.cmet.2023.02.005.
16. Kliewer, S.A., and Mangelsdorf, D.J. (2019). A dozen years of discovery: insights into the physiology and pharmacology of FGF21. Cell Metab. *29*, 246–253. https://doi.org/10.1016/j.cmet.2019.01.004.
17. Lundsgaard, A.M., Fritzen, A.M., Sjøberg, K.A., Myrmel, L.S., Madsen, L., Wojtaszewski, J.F.P., Richter, E.A., and Kiens, B. (2017). Circulating FGF21 in humans is potently induced by short term overfeeding of carbohydrates. Mol. Metab. *6*, 22–29. https://doi.org/10.1016/j.molmet.2016.11.001.
18. De Sousa-Coelho, A.L., Marrero, P.F., and Haro, D. (2012). Activating transcription factor 4-dependent induction of FGF21 during amino acid deprivation. Biochem. J. *443*, 165–171. https://doi.org/10.1042/bj20111748.
19. Schaap, F.G., Kremer, A.E., Lamers, W.H., Jansen, P.L.M., and Gaemers, I.C. (2013). Fibroblast growth factor 21 is induced by endoplasmic reticulum stress. Biochimie *95*, 692–699. https://doi.org/10.1016/j.biochi.2012.10.019.
20. Jiang, S., Yan, C., Fang, Q.C., Shao, M.L., Zhang, Y.L., Liu, Y., Deng, Y.P., Shan, B., Liu, J.Q., Li, H.T., et al. (2014). Fibroblast growth factor 21 is regulated by the IRE1α-XBP1 branch of the unfolded protein response and counteracts endoplasmic reticulum stress-induced hepatic steatosis. J. Biol. Chem. *289*, 29751–29765. https://doi.org/10.1074/jbc.M114.565960.
21. Hetz, C., Zhang, K., and Kaufman, R.J. (2020). Mechanisms, regulation and functions of the unfolded protein response. Nat. Rev. Mol. Cell Biol. *21*, 421–438. https://doi.org/10.1038/s41580-020-0250-z.
22. Pakos-Zebrucka, K., Koryga, I., Mnich, K., Ljujic, M., Samali, A., and Gorman, A.M. (2016). The integrated stress response. EMBO Rep. *17*, 1374–1395. https://doi.org/10.15252/embr.201642195.
23. Donnelly, N., Gorman, A.M., Gupta, S., and Samali, A. (2013). The eIF2α kinases: their structures and functions. Cell. Mol. Life Sci. *70*, 3493–3511. https://doi.org/10.1007/s00018-012-1252-6.
24. Dong, K., Li, H., Zhang, M., Jiang, S., Chen, S., Zhou, J., Dai, Z., Fang, Q., and Jia, W. (2015). Endoplasmic reticulum stress induces up-regulation of hepatic β-Klotho expression through ATF4 signaling pathway. Biochem. Biophys. Res. Commun. *459*, 300–305. https://doi.org/10.1016/j.bbrc.2015.02.104.
25. Maruyama, R., Shimizu, M., Hashidume, T., Inoue, J., Itoh, N., and Sato, R. (2018). FGF21 alleviates hepatic endoplasmic reticulum stress under physiological conditions. J. Nutr. Sci. Vitaminol. (Tokyo) *64*, 200–208. https://doi.org/10.3177/jnsv.64.200.
26. Kharitonenkov, A., Shiyanova, T.L., Koester, A., Ford, A.M., Micanovic, R., Galbreath, E.J., Sandusky, G.E., Hammond, L.J., Moyers, J.S., Owens, R.A., et al. (2005). FGF-21 as a novel metabolic regulator. J. Clin. Investig. *115*, 1627–1635. https://doi.org/10.1172/jci23606.
27. Lee, S., Choi, J., Mohanty, J., Sousa, L.P., Tome, F., Pardon, E., Steyaert, J., Lemmon, M.A., Lax, I., and Schlessinger, J. (2018). Structures of β-klotho reveal a 'zip code'-like mechanism for endocrine FGF signalling. Nature *553*, 501–505. https://doi.org/10.1038/nature25010.
28. Minard, A.Y., Tan, S.X., Yang, P., Fazakerley, D.J., Domanova, W., Parker, B.L., Humphrey, S.J., Jothi, R., Stöckli, J., and James, D.E. (2016). mTORC1 is a major regulatory node in the FGF21 signaling network in adipocytes. Cell Rep. *17*, 29–36. https://doi.org/10.1016/j.celrep.2016.08.086.
29. Hosoki, R., Matsuki, N., and Kimura, H. (1997). The possible role of hydrogen sulfide as an endogenous smooth muscle relaxant in synergy with nitric oxide. Biochem. Biophys. Res. Commun. *237*, 527–531. https://doi.org/10.1006/bbrc.1997.6878.
30. Zhao, W., Zhang, J., Lu, Y., and Wang, R. (2001). The vasorelaxant effect of H(2)S as a novel endogenous gaseous K(ATP) channel opener. EMBO J. *20*, 6008–6016. https://doi.org/10.1093/emboj/20.21.6008.

31. Yang, G., Wu, L., Jiang, B., Yang, W., Qi, J., Cao, K., Meng, Q., Mustafa, A.K., Mu, W., Zhang, S., et al. (2008). H2S as a physiologic vasorelaxant: hypertension in mice with deletion of cystathionine gamma-lyase. Science *322*, 587–590. https://doi.org/10.1126/science.1162667.

32. Mustafa, A.K., Gadalla, M.M., Sen, N., Kim, S., Mu, W., Gazi, S.K., Barrow, R.K., Yang, G., Wang, R., and Snyder, S.H. (2009). H2S signals through protein S-sulfhydration. Sci. Signal. *2*, ra72. https://doi.org/10.1126/scisignal.2000464.

33. Toohey, J.I. (2011). Sulfur signaling: is the agent sulfide or sulfane? Anal. Biochem. *413*, 1–7. https://doi.org/10.1016/j.ab.2011.01.044.

34. Filipovic, M.R., Zivanovic, J., Alvarez, B., and Banerjee, R. (2018). Chemical biology of H2S signaling through persulfidation. Chem. Rev. *118*, 1253–1337. https://doi.org/10.1021/acs.chemrev.7b00205.

35. Mishanina, T.V., Libiad, M., and Banerjee, R. (2015). Biogenesis of reactive sulfur species for signaling by hydrogen sulfide oxidation pathways. Nat. Chem. Biol. *11*, 457–464. https://doi.org/10.1038/nchembio.1834.

36. Cirino, G., Szabo, C., and Papapetropoulos, A. (2023). Physiological roles of hydrogen sulfide in mammalian cells, tissues, and organs. Physiol. Rev. *103*, 31–276. https://doi.org/10.1152/physrev.00028.2021.

37. Ida, T., Sawa, T., Ihara, H., Tsuchiya, Y., Watanabe, Y., Kumagai, Y., Suematsu, M., Motohashi, H., Fujii, S., Matsunaga, T., et al. (2014). Reactive cysteine persulfides and S-polythiolation regulate oxidative stress and redox signaling. Proc. Natl. Acad. Sci. USA *111*, 7606–7611. https://doi.org/10.1073/pnas.1321232111.

38. Akaike, T., Ida, T., Wei, F.Y., Nishida, M., Kumagai, Y., Alam, M.M., Ihara, H., Sawa, T., Matsunaga, T., Kasamatsu, S., et al. (2017). Cysteinyl-tRNA synthetase governs cysteine polysulfidation and mitochondrial bioenergetics. Nat. Commun. *8*, 1177. https://doi.org/10.1038/s41467-017-01311-y.

39. Lam, S.S., Martell, J.D., Kamer, K.J., Deerinck, T.J., Ellisman, M.H., Mootha, V.K., and Ting, A.Y. (2015). Directed evolution of APEX2 for electron microscopy and proximity labeling. Nat. Methods *12*, 51–54. https://doi.org/10.1038/nmeth.3179.

40. Asimakopoulou, A., Panopoulos, P., Chasapis, C.T., Coletta, C., Zhou, Z., Cirino, G., Giannis, A., Szabo, C., Spyroulias, G.A., and Papapetropoulos, A. (2013). Selectivity of commonly used pharmacological inhibitors for cystathionine β synthase (CBS) and cystathionine γ lyase (CSE). Br. J. Pharmacol. *169*, 922–932. https://doi.org/10.1111/bph.12171.

41. Kabil, O., Vitvitsky, V., Xie, P., and Banerjee, R. (2011). The quantitative significance of the transsulfuration enzymes for H2S production in murine tissues. Antioxid. Redox Signal. *15*, 363–372. https://doi.org/10.1089/ars.2010.3781.

42. Huang, S., Xing, Y., and Liu, Y. (2019). Emerging roles for the ER stress sensor IRE1α in metabolic regulation and disease. J. Biol. Chem. *294*, 18726–18741. https://doi.org/10.1074/jbc.REV119.007036.

43. Madhavan, A., Kok, B.P., Rius, B., Grandjean, J.M.D., Alabi, A., Albert, V., Sukiasyan, A., Powers, E.T., Galmozzi, A., Saez, E., et al. (2022). Pharmacologic IRE1/XBP1s activation promotes systemic adaptive remodeling in obesity. Nat. Commun. *13*, 608. https://doi.org/10.1038/s41467-022-28271-2.

44. Krishnan, N., Fu, C., Pappin, D.J., and Tonks, N.K. (2011). H2S-induced sulfhydration of the phosphatase PTP1B and its role in the endoplasmic reticulum stress response. Sci. Signal. *4*, ra86. https://doi.org/10.1126/scisignal.2002329.

45. Yadav, V., Gao, X.H., Willard, B., Hatzoglou, M., Banerjee, R., and Kabil, O. (2017). Hydrogen sulfide modulates eukaryotic translation initiation factor 2α (eIF2α) phosphorylation status in the integrated stress-response pathway. J. Biol. Chem. *292*, 13143–13153. https://doi.org/10.1074/jbc.M117.778654.

46. Coate, K.C., Hernandez, G., Thorne, C.A., Sun, S., Le, T.D.V., Vale, K., Kliewer, S.A., and Mangelsdorf, D.J. (2017). FGF21 is an exocrine pancreas secretagogue. Cell Metab. *25*, 472–480. https://doi.org/10.1016/j.cmet.2016.12.004.

47. Dickhout, J.G., Carlisle, R.E., Jerome, D.E., Mohammed-Ali, Z., Jiang, H., Yang, G., Mani, S., Garg, S.K., Banerjee, R., Kaufman, R.J., et al. (2012). Integrated stress response modulates cellular redox state via induction of cystathionine γ-lyase: cross-talk between integrated stress response and thiol metabolism. J. Biol. Chem. *287*, 7603–7614. https://doi.org/10.1074/jbc.M111.304576.

48. Yang, L.-X., Qi, C., Lu, S., Ye, X.-S., Merikhian, P., Zhang, D.-Y., Yao, T., Zhao, J.-S., Wu, Y., Jia, Y., et al. (2025). Alleviation of liver fibrosis by inhibiting a non-canonical ATF4-regulated enhancer program in hepatic stellate cells. Nat. Commun. *16*, 524. https://doi.org/10.1038/s41467-024-55738-1.

49. He, F., Zhang, P., Liu, J., Wang, R., Kaufman, R.J., Yaden, B.C., and Karin, M. (2023). ATF4 suppresses hepatocarcinogenesis by inducing SLC7A11 (xCT) to block stress-related ferroptosis. J. Hepatol. *79*, 362–377. https://doi.org/10.1016/j.jhep.2023.03.016.

50. Kabil, O., Yadav, V., and Banerjee, R. (2016). Heme-dependent metabolite switching regulates H2S synthesis in response to endoplasmic reticulum (ER) stress. J. Biol. Chem. *291*, 16418–16423. https://doi.org/10.1074/jbc.C116.742213.

51. Gao, X.H., Krokowski, D., Guan, B.J., Bederman, I., Majumder, M., Parisien, M., Diatchenko, L., Kabil, O., Willard, B., Banerjee, R., et al. (2015). Quantitative H2S-mediated protein sulfhydration reveals metabolic reprogramming during the integrated stress response. eLife *4*, e10067. https://doi.org/10.7554/eLife.10067.

52. Tezze, C., Romanello, V., Desbats, M.A., Fadini, G.P., Albiero, M., Favaro, G., Ciciliot, S., Soriano, M.E., Morbidoni, V., Cerqua, C., et al. (2017). Age-associated loss of OPA1 in muscle impacts muscle mass, metabolic homeostasis, systemic inflammation, and epithelial senescence. Cell Metab. *25*, 1374–1389.e6. https://doi.org/10.1016/j.cmet.2017.04.021.

53. Hine, C., Harputlugil, E., Zhang, Y., Ruckenstuhl, C., Lee, B.C., Brace, L., Longchamp, A., Treviño-Villarreal, J.H., Mejia, P., Ozaki, C.K., et al. (2015). Endogenous hydrogen sulfide production is essential for dietary restriction benefits. Cell *160*, 132–144. https://doi.org/10.1016/j.cell.2014.11.048.

54. Hine, C., Kim, H.J., Zhu, Y., Harputlugil, E., Longchamp, A., Matos, M.S., Ramadoss, P., Bauerle, K., Brace, L., Asara, J.M., et al. (2017). Hypothalamic-pituitary axis regulates hydrogen sulfide production. Cell Metab. *25*, 1320–1333.e5. https://doi.org/10.1016/j.cmet.2017.05.003.

55. Zhang, Y., Xie, Y., Berglund, E.D., Coate, K.C., He, T.T., Katafuchi, T., Xiao, G., Potthoff, M.J., Wei, W., Wan, Y., et al. (2012). The starvation hormone, fibroblast growth factor-21, extends lifespan in mice. eLife *1*, e00065. https://doi.org/10.7554/eLife.00065.

56. Gliniak, C.M., Gordillo, R., Youm, Y.H., Lin, Q., Crewe, C., Zhang, Z., Field, B.C., Fujikawa, T., Virostek, M., Zhao, S., et al. (2025). FGF21 promotes longevity in diet-induced obesity through metabolic benefits independent of growth suppression. Cell Metab. *37*, 1547–1567.e6. https://doi.org/10.1016/j.cmet.2025.05.011.

57. Rose, J.P., Morgan, D.A., Sullivan, A.I., Fu, X., Inigo-Vollmer, M., Burgess, S.C., Meyerholz, D.K., Rahmouni, K., and Potthoff, M.J. (2025). FGF21 reverses MASH through coordinated actions on the CNS and liver. Cell Metab. *37*, 1515–1529.e6. https://doi.org/10.1016/j.cmet.2025.04.014.

58. Zivanovic, J., Kouroussis, E., Kohl, J.B., Adhikari, B., Bursac, B., Schott-Roux, S., Petrovic, D., Miljkovic, J.L., Thomas-Lopez, D., Jung, Y., et al. (2019). Selective persulfide detection reveals evolutionarily conserved antiaging effects of S-sulfhydration. Cell Metab. *30*, 1152–1170.e13. https://doi.org/10.1016/j.cmet.2019.10.007.

59. Cáliz-Molina, M.Á., López-Fernández-Sobrino, R., Pino-Pérez, I., Panadero-Morón, C., Vilches-Pérez, M.D.C., Camacho-Cabrera, M., García-Ruiz, A., Pérez-Rosendo, L., Espadas, I., Sola-García, A., et al. (2025). Enhanced non-enzymatic H2S generation extends lifespan and healthspan in male mice. Cell Metab. *38*, 350–369.e8. https://doi.org/10.1016/j.cmet.2025.11.012.

60. Perez-Riverol, Y., Bai, J., Bandla, C., García-Seisdedos, D., Hewapathirana, S., Kamatchinathan, S., Kundu, D.J., Prakash, A., Frericks-Zipper, A., Eisenacher, M., et al. (2022). The PRIDE database resources in 2022: a hub for mass spectrometry-based proteomics

evidences. Nucleic Acids Res. *50*, D543–D552. https://doi.org/10.1093/nar/gkab1038.

61. Hotta, Y., Nakamura, H., Konishi, M., Murata, Y., Takagi, H., Matsumura, S., Inoue, K., Fushiki, T., and Itoh, N. (2009). Fibroblast growth factor 21 regulates lipolysis in white adipose tissue but is not required for ketogenesis and triglyceride clearance in liver. Endocrinology *150*, 4625–4633. https://doi.org/10.1210/en.2009-0119.
62. Ding, X., Boney-Montoya, J., Owen, B.M., Bookout, A.L., Coate, K.C., Mangelsdorf, D.J., and Kliewer, S.A. (2012). βKlotho is required for fibroblast growth factor 21 effects on growth and metabolism. Cell Metab. *16*, 387–393. https://doi.org/10.1016/j.cmet.2012.08.002.
63. Grosche, A., Hauser, A., Lepper, M.F., Mayo, R., von Toerne, C., Merl-Pham, J., and Hauck, S.M. (2016). The proteome of native adult müller glial cells from murine retina. Mol. Cell. Proteomics *15*, 462–480. https://doi.org/10.1074/mcp.M115.052183.
64. Wiśniewski, J.R., Zougman, A., Nagaraj, N., and Mann, M. (2009). Universal sample preparation method for proteome analysis. Nat. Methods *6*, 359–362. https://doi.org/10.1038/nmeth.1322.
65. Navarro, P., Trevisan-Herraz, M., Bonzon-Kulichenko, E., Núñez, E., Martínez-Acedo, P., Pérez-Hernández, D., Jorge, I., Mesa, R., Calvo, E., Carrascal, M., et al. (2014). General statistical framework for quantitative proteomics by stable isotope labeling. J. Proteome Res. *13*, 1234–1247. https://doi.org/10.1021/pr4006958.
66. Hine, C., and Mitchell, J.R. (2017). Endpoint or kinetic measurement of hydrogen sulfide production capacity in tissue extracts. Bio Protoc. *7*, e2382. https://doi.org/10.21769/BioProtoc.2382.
67. Schindelin, J., Arganda-Carreras, I., Frise, E., Kaynig, V., Longair, M., Pietzsch, T., Preibisch, S., Rueden, C., Saalfeld, S., Schmid, B., et al. (2012). Fiji: an open-source platform for biological-image analysis. Nat. Methods *9*, 676–682. https://doi.org/10.1038/nmeth.2019.

Please cite this article in press as: Grandl et al., FGF21 reduces ER stress by enhancing the unfolded protein and integrated stress responses through increased sulfide signaling, Cell Metabolism (2026), https://doi.org/10.1016/j.cmet.2026.05.011

STAR★METHODS

KEY RESOURCES TABLE

REAGENT or RESOURCE	SOURCE	IDENTIFIER
Antibodies		
XBP-1s (D2C1F) Rabbit mAb	Cell Signaling Technology	12782; RRID: AB_2687943
Anti-EIF2S1 (phospho S51) antibody [E90] rabbit	abcam	ab32157; RRID: AB_732117
EIF2S1 Monoclonal Antibody (EIF2-alpha) mouse	Invitrogen ThermoFisher	AHO0802; RRID: AB_1500037
eIF2 alpha Antibody Rabbit	Cell Signaling Technology	9722; RRID: AB_2230924
p-ERK1/2 Antibody Rabbit mAb	Cell Signaling Technology	9101; RRID: AB_331646
ERK1/2 Antibody Mouse mAb	Cell Signaling Technology	4696; RRID: AB_390780
CBS (D8F2P) Rabbit mAb	Cell Signaling Technology	14782; RRID: AB_2798609
Cystathionine γ-Lyase (D1N1D) Rabbit mAb	Cell Signaling Technology	19689; RRID: AB_2798824
ATF-4 (D4B8) Rabbit Monoclonal Antibody	Cell Signaling Technology	11815; RRID: AB_2616025
Anti KLB middle region Rabbit	Aviva Systems Biology	ARP53325_P050; RRID: AB_10640493
CTH monoclonal antibody (M03), clone S51 Mouse	Abnova	H00001491-M03
Monocolonal Anti Flag M2 Mouse Ab	SIGMA	F1804; RRID: AB_538058
Mouse Anti -Rabbit HRP	Helmholtz AB Core Facility	N/A
StarBright Blue 700 Goat Anti-Rabbit IgG	Bio-Rad Laboratories	12004161; RRID: AB_2721073
StarBright Blue 700 Goat Anti-Mouse IgG	Bio-Rad Laboratories	12005867; RRID: AB_3712169
StarBright Blue 520 Goat Anti-Mouse IgG	Bio-Rad Laboratories	12005866; RRID: AB_2934034
Donkey Anti-Mouse IgG H&L (Alexa Fluor 790)	abcam	ab175782
α-Tubulin (DM1A) Mouse mAb	Cell Signaling Technology	3873; RRID: AB_1904178
β-Actin mouse mAb	Cell Signaling Technology	3700; RRID: AB_2242334
β-Actin HRP mouse monoclonal IgG	Santa Cruz Biotechnology	sc-47778; RRID: AB_626632
Bacterial and virus strains		
AAV-TBG-eGFP	vector biolabs	VB1743
AAV-TBG-iCre	vector biolabs	VB1724
Chemicals, peptides, and recombinant proteins		
FGF21 (human)	Novo Nordisk Indiana	N/A
SulfoBiotics- SSP4	Dojindo	1810731-98-6
Tunicamycin Mixture	Cayman Chemicals	11445
GYY 4137	Cayman Chemicals	13345
(Aminooxy)acetic acid	Sigma	c13408
DL propargylglycine	Sigma	P7888
Dynabeads M-280 Streptavidin	Invitrogen ThermoFisher	11205D
StrepTactin-HRP Conjugate	Bio-Rad Laboratories	1610381
Biotinyl tyramide	Biomol	CDX-B0270-M500
Critical commercial assays		
Mouse/Rat FGF-21 Quantikine ELISA Kit	R&D Systems	MF2100
Duolink Proximity Ligation Assay	Sigma-Aldrich	DUO92101
Deposited data		
Proteomics data deposited to PRIDE	This paper	PRIDE: PXD056693
Source Data	This paper	Data S1
Experimental models: Cell lines		
KLBAPEX cells, based on Flp-In T-REx 293	This paper	N/A
APEX cells, based on Flp-In T-REx 293	This paper	N/A
Human embryonic kidney (HEK) Flp-In T-Rex 293	Invitrogen ThermoFisher	R78007

(*Continued on next page*)

Please cite this article in press as: Grandl et al., FGF21 reduces ER stress by enhancing the unfolded protein and integrated stress responses through increased sulfide signaling, Cell Metabolism (2026), https://doi.org/10.1016/j.cmet.2026.05.011

CellPress
OPEN ACCESS

Continued

REAGENT or RESOURCE	SOURCE	IDENTIFIER
Experimental models: Organisms/strains		
FGF21KO mice	Hotta et al.[61]	N/A
$Cth^{tm1a(EUCOMM)Hmgu}$ mice	Infrafrontier	EM:09267
B6.129S4-*Gt(ROSA)26Sor*^{tm1Sor}/J	The Jackson Laboratory	JAX:003474
B6.129S6(SJL)-*Klb*$^{tm1.1Sakl}$/J	The Jackson Laboratory	JAX:026883
Oligonucleotides		
ON-TARGETplus Human CBS siRNA	Dharmacon	L-008617-00-0005
ON-TARGETplus Human CTH siRNA	Dharmacon	L-003481-00-0005
ON-TARGETplus Non-targeting Control Pool	Dharmacon	D-001810-10-20
36B4 mouse fw: AACGGCAGCATTTATAACCC, rev: CGATCTGCAGACACACACTG	This study, synthesized by SIGMA	N/A
Atf4 mouse fw: GATGAGCTTCCTGAACAGCG, rev: GCCAAGCCATCATCCATAGC	This study, synthesized by SIGMA	N/A
Klb mouse fw: ACACAACCTGATCAAGGCACA, rev: GTCTGGCGTGGACTCTTTCA	This study, synthesized by SIGMA	N/A
Xbp1s mouse fw: GGTCTGCTGAGTCCGCAGCAGG, rev: AGGCTTGGTGTATACATGG	This study, synthesized by SIGMA	N/A
Ddit3 mouse fw: CCACCACACCTGAAAGCAGAA, rev: AGGTGAAAGGCAGGGACTCA	This study, synthesized by SIGMA	N/A
Xbp1s human fw: CTGAGTCCGAATCAGGTGCAG, rev: ATCCATGGGGAGATGTTCTGG	This study, synthesized by SIGMA	N/A
Tbp human fw: AACAACAGCCTGCCACCTTA, rev: GCCATAAGGCATCATTGGAC	This study, synthesized by SIGMA	N/A
Recombinant DNA		
pcDNA 5/FRT Mammalian Expression Vector	Invitrogen ThermoFisher	V601020
pcDNA KLB-APEX (based on pcDNA3.1)	This study	N/A
pcDNA APEX (based on pcDNA3.1)	This study	N/A
Software and algorithms		
GraphPad Prism 9.0	GraphPad	N/A
GraphPad Prism 10.0	GraphPad	N/A
ImageJ / FIJI	NIH Image	N/A
Proteome Discoverer	ThermoFisher Scientific	version 2.3.0.523

EXPERIMENTAL MODEL AND STUDY PARTICIPANT DETAILS

Animals and housing conditions

Animal experiments were performed in accordance with the Animal Protection Law of the European Union, and upon permission by the state of Bavaria, Germany. Only male mice were used for the studies except for the viral liver-specific KLBKO which was performed in female mice due to availability. Mice were group-housed on a 12:12 hour light-dark cycle at 22 ± 1 °C with free access to food and water unless indicated otherwise. C57BL/6J mice were provided by Janvier Labs. CTHKO mice were generated by crossing $Cth^{tm1a(EUCOMM)Hmgu}$, where the critical exon 2 is flanked by two Loxp sites, into Rosa26-CRE mice and back-crossed into C57BL/6J. FGF21KO animals generated by targeted deletion of exons 1–3, were generously provided by N. Itoh,[61] and back-crossed into C57BL/6J. Liver specific KLBKO animals were generated in mice carrying a floxed KLB allele (Jackson #026883)[62] by retroorbital delivery of AAV8-TGB-Cre (KO) or AAV8-eGFP (WT). Mice were injected with 1mg/kg FGF21 (human, a gift from Novo Nordisk), 1mg/kg tunicamycin (Tm, Cayman), their combination (1mg/kg each in the same injection), or vehicle subcutaneously (s.c). in phosphate buffered saline. For short term studies, FGF21 injections were performed either acutely (4h before sacrifice) or with an additional FGF21 injection the evening before sacrifice. Tm injections (with FGF21 or alone) were always done acutely (4h before sacrifice). The H_2S-donor GYY4137 was administered via 2 s.c. injections, one in the evening, and the second the following morning 4h prior to sacrifice. The GYY4137 dose was 100mg/kg for the pilot study and 200mg/kg for the gain of function experiment with Tm and FGF21. For chronic FGF21 injections animals were injected with 100nmol/kg (approximately 2mg/kg) s.c. once daily for 2 weeks with FGF21 or vehicle. Glucose tolerance test was performed by injecting 1.75g glucose/kg i.p. and insulin tolerance test was performed by injecting 0.75mU insulin/kg i.p., blood glucose was measured by tail vein punction.

Please cite this article in press as: Grandl et al., FGF21 reduces ER stress by enhancing the unfolded protein and integrated stress responses through increased sulfide signaling, Cell Metabolism (2026), https://doi.org/10.1016/j.cmet.2026.05.011

Cell culture

Human embryonic kidney (HEK) Flp-In T-REx 293 cells with stable overexpression of β-klotho-APEX2 or APEX2 were cultivated in DMEM with 10% FBS and 0.2% hygromycin B at 37°C with 95% humidity and 5 % CO2. For transgene induction doxycycline (1μg/ml) was added. Cells were treated with 5 nM FGF21 and 0.2 μg/ml or 0.05 μg/ml Tunicamycin (Tm). siRNAs (Dharmacon) were transfected using lipofectamine 3000 (Invitrogen), and experiments were started 24h after siRNA transfection. Amino-oxoacetic acid (AOA, 0,5mM) was co-administered with vehicle, FGF21 or FGF21 + Tm for 4 h. Sulfane sulfur was measured using the fluorescent probe SSP4 (Dojindo Bio). After o/n treatment with FGF21, Tm, or serum starvation, cells were incubated with 10uM SSP4 in serum free medium for 30 minutes at 37°C and fluorescence was measured at an excitation wavelength of 482 nm and emission wavelength of 515 nm.

METHOD DETAILS

APEX2 labelling and biotin pulldown

Confluent 10cm dishes of cells were incubated with 500μM biotin-phenol (Biomol CDX-B0270-M500) in serum free DMEM for 1h. FGF21 was added to 5nM for the appropriate time. For the last 30 seconds H_2O_2 was added to 1mM. The medium was immediately poured out and aspirated and the cells flushed off the plate with quenching buffer (PBS with 10 mM sodium ascorbate, 10 mM sodium azide, 5 mM trolox). $1/10^{th}$ of the cell suspension was separated, washed with PBS and used for protein estimation (BCA assay, Pierce). After 3 washes with quenching buffer, samples were resuspended in lysis buffer (6 M urea, 0.3 M NaCl, 1 mM EDTA, 25 mM Tris/HCl pH 7.5, 1%SDS, 10 mM sodium ascorbate, 10 mM sodium azide, 5 mM trolox, with protease/phosphatase inhibitors (Halt)), and frozen at -80°C. For biotin pulldown 100μl of Dynabeads (Invitrogen M-280 streptavidin) per sample were incubated with 400μg of protein for 1h at RT on a rotary shaker. Beads were pelleted using a magnetic rack and washed for 10min in 1 ml 50mM DTT in 1% SDS (50mM Tris, pH 7.4) on a rotary shaker and then 2 times in 1% SDS, 3 times in RIPA (Sigma) and 3 times in 4M urea (50mM Tris, pH 7.4), 1ml each, by resuspension. Samples were eluted in 50mM Tris pH 6.8, 1% SDS, 2mM biotin at 65°C in a rotary shaker. A full list of the identified proteins is available in Table S1.

Filter aided sample preparation (FASP) digest

Samples were digested using a modified FASP procedure.[63,64] After protein reduction and alkylation using DTT and IAA, the proteins were centrifuged on a 30 kDa cutoff filter device (Sartorius), washed thrice with UA buffer (8 M urea in 0.1 M Tris/HCl pH 8.5) and twice with 50 mM ABC. The proteins were digested for 2 hours at room temperature using 0.5 μg Lys-C (Wako Chemicals, Neuss, Germany) and for 16 hours at 37°C using 1 μg trypsin (Promega, Mannheim, Germany). After centrifugation (10 min at 14 000 g) the eluted peptides were acidified with 0.5% TFA and stored at -20°C.

LC-MSMS measurements

LC-MS/MS analysis was performed on a Q-Exactive HF mass spectrometer (Thermo Scientific) online coupled to an Ultimate 3000 nano-RSLC (Thermo Scientific). Tryptic peptides were automatically loaded on a C18 trap column (300 μm inner diameter (ID) × 5 mm, Acclaim PepMap100 C18, 5 μm, 100 Å, LC Packings) at 30μl/min flow rate prior to C18 reversed phase chromatography on the analytical column (nanoEase MZ HSS T3 Column, 100Å, 1.8 μm, 75 μm x 250 mm, Waters) at 250nl/min flow rate in a 95 minutes non-linear acetonitrile gradient from 3% to 40% in 0.1% formic acid. Profile precursor spectra from 300 to 1500 m/z were recorded at 60000 resolution with an automatic gain control (AGC) target of 3e6 and a maximum injection time of 30 ms. TOP10 fragment spectra of charges 2 to 7 were recorded at 15000 resolution with an AGC target of 1e5, a maximum injection time of 50 ms, an isolation window of 1.6 m/z, a normalized collision energy of 28 and a dynamic exclusion of 30 seconds. The mass spectrometry proteomics data have been deposited to the ProteomeXchange Consortium via the PRIDE[60] partner repository with the dataset identifier PRIDE: PXD056693.

Protein identification and label-free quantification

Proteome Discoverer software (Thermo Fisher Scientific; version 2.3.0.523; 2.4.1.15) was used for peptide and protein identification via a database search (Sequest HT search engine) against Swissprot Human data base (Release 2020_02, 20432 sequences), considering full tryptic specificity, allowing for up to two missed tryptic cleavage sites, precursor mass tolerance 10 ppm, fragment mass tolerance 0.02 Da. Carbamidomethylation of Cys was set as a static modification. Dynamic modifications included deamidation of Asn, Gln and Arg, oxidation of Pro and Met; and a combination of Met loss with acetylation on protein N-terminus. Percolator was used for validating peptide spectrum matches and peptides, accepting only the top-scoring hit for each spectrum, and satisfying the cutoff values for FDR <5%, and posterior error probability <0.01. The final list of proteins complied with the strict parsimony principle.

The quantification of proteins was based on top three most abundant unique peptides. Abundance values were normalized on total peptide amount to account for sample loading errors. The protein abundances were calculated summing up the abundance values for admissible peptides. The final protein ratio was calculated using median abundance values. The statistical significance of the ratio change was ascertained employing the T-test approach described in Navarro et al.[65] which is based on the presumption that we look for expression changes for proteins that are just a few in comparison to the number of total proteins being quantified. The quantification variability of the non-changing "background" proteins can be used to infer which proteins change their expression in a

statistically significant manner. For GO-term overrepresentation test, the accession numbers of detected proteins with an abundance ratio >1.4 in at least one of the FGF21-treated time-points were used, against a database of the complete human proteome.

Western blot

Cell culture samples were lysed in RIPA buffer (sigma) with protease/phosphatase inhibitors for 30min on ice, sonicated in ice cold water, centrifuged (15000g, 15 min, 4 °C) and supernatant collected. Protein concentration was estimated using a BCA assay (Pierce). Liver samples were prepared in passive lysis buffer as described for the H_2S-production measurements. Samples were diluted in 4x loading buffer (NuPAGE) supplemented with 50mM DTT and heated to 95°C for 10min. SDS-PAGE was performed using the Criterion TGX system (Biorad) on 4%–20% bisacrylamide gradient gels. Proteins were transferred to nitrocellulose or PVDF membranes using the Trans-Blot Turbo Transfer system. Membranes were blocked in 5% milk in TBST, or Roti-Block. Fluorescent secondary antibodies, or antibodies fused to horse radish peroxidase (HRP), detected with Amersham ECL Select (RPN2235), were used. Membranes were imaged on a ChemiDoc imaging system (Biorad). Densitometric analysis was performed using the ImageLab software (Biorad). A complete list of antibodies used is provided in the supplemental information.

H_2S-production measurements from liver extracts

H_2S measurements were based on a protocol by Hine and Mitchell.[66] Approximately 100mg of frozen liver tissue was homogenized in 200ul of passive lysis buffer (Promega) using a tungsten bead in a Tissue Lyser II (Quiagen). Samples were subjected to 3 freeze thaw cycles in liquid nitrogen and a 37°C shaker, centrifuged for 10 min at 15000g at 4°C and the supernatant collected. Protein concentration was estimated using a BCA assay (Pierce). 100–200 μg of protein was incubated with PBS with 10mM L-cysteine and 1mM Pyridoxale phosphate at 37°C in a 96 well plate covered with a filter paper that had been soaked in lead-acetate and dried. Staining was checked every hour and filter papers were removed after 2–3h and imaged on a ChemiDoc imaging system (Biorad). Densitometric analysis of lead-acetate staining was performed using the ImageLab software (Biorad).

Persulfide quantification in fresh liver slices

Fresh mouse livers were sliced on a vibratome in Krebs ringer buffer on ice with a thickness of 200um. 5mm circular discs were punched from liver slices and incubated at 37°C in oxygenated phenol-red-free Williams' E medium (Gibco, A1217601) containing 10% FBS, glutamate (2 mM), and penicillin-streptomycin for 2h. Slices were treated with 500nM FGF21, 10μg/ml tunicamycin, or vehicle together with 1μM of the sulfane sulfur probe SSP4 overnight. SSP4 fluorescence was measured after 16 to 18 hours on a Varioskan plate reader (Thermo Fisher) at an excitation wavelength of 482nm and emission at 515nm.

Proximity ligation assay

Mice were treated with 1mg/kg FGF21 or PBS twice, 16h and 4h prior to cervical dislocation and intracardiac perfusion with ice-cold TBS, followed by fixative (Roti-Histofix, P087.1). Livers were postfixed, dehydrated in a sucrose gradient (15%, 30%) and cryosectioned into 10 μm sections mounted on slides. The slides were used for immunodetection using primary antibodies anti-KLB (1:100, ARP53325_P050, Aviva) and anti-CTH (1:300, H00001491-M03, Abnova) overnight at 4°C. Proximity ligation was performed using Duolink reagents (Sigma-Aldrich, DUO92101) according to the manufacturer's protocol and imaged on a Leica Stellaris 8 (Leica Microsystems) laser scanning confocal microscope. Fluorescence signals were automatically counted using Fiji software.[67]

Gene expression analysis

RNA was extracted using RNeasy Mini Kits (Qiagen). cDNA was generated with QuantiTech reverse transcription kit (Qiagen). Quantitative PCR (qPCR) was performed with a ViiA 7 PCR System (Applied Biosystems) Using Syber Green (prod). Target gene expression was normalized to reference gene 36B4 by ΔΔCT. A complete list of used primers is available in the supplemental information.

QUANTIFICATION AND STATISTICAL ANALYSIS

Statistical analyses were conducted using the statistical tools implemented in GraphPad Prism. Statistical significance was determined using unpaired 2-tailed Student's t test, one-way ANOVA, two-way or three-way ANOVA, followed by appropriate post hoc test as indicated in the figure legends. $P \leq 0.05$ was considered statistically significant.